Results

We first constructed the retroviral vector system in which the gene for MazF was inserted downstream of the HIV-1 TAR sequence (Fig. 1). As the *E. coli mazF* gene contains nine ACA sequences in its open-reading frame, all of these ACA sequences were first engineered to other MazF-uncleavable sequences without altering the amino acid sequence of MazF to make the *mazF* mRNA resistant to MazF. The resulting self-inactivating retroviral vector (MTD3-U3TAR-MazF) was used to transduce CD4+ T lymphoid CEM-SS cells to create a system in which MazF induction in CEM-SS cells upon infection with HIV-1 effectively suppressed HIV-1 replication without causing apoptosis of infected T cells. The MTD3 retroviral vector contained an intact 5′ LTR and a mutated 3′ LTR that lacks most of the transcriptional elements present in U3. Cells transduced with the resulting retroviral vector contained the defective LTR at both ends (Yu *et al.*, 1986). The self-inactivating retroviral vector was transiently produced and subsequently transduced into the human T lymphoid line CEM-SS cells, which are highly susceptible to HIV infection. Transduced cells were subjected to G418 selection to obtain drug-resistant populations. A GFP-expressing retroviral vector under the control of HIV-LTR (MTD3-U3TAR-GFP) was also used as a control.

The growth rate of CEM-SS cells transduced with MTD3-U3TAR-MazF was comparable to that of the parental CEM-SS line (Fig. 2A), suggesting that MazF expression was tightly controlled and did not inhibit cell growth. Furthermore, the CD4 levels of MTD3-U3TAR-MazF-transduced CEM-SS cells were identical to those of the parental CEM-SS cells (Fig. 3A).

To investigate the effects of HIV-1 infection, MazF-transduced or GFP-transduced CEM-SS cells were infected with HIV-1 IIIB at different MOIs, specifically 0.07, 0.0007, and 0.00007 (Fig. 4). Levels of the HIV-1 p24 antigen in the culture media were examined 16 days post infection. As shown in Fig. 4, in MazF-transduced CEM-SS cells, HIV-1 replication was effectively suppressed. To more precisely investigate the antiviral effects of MazF, viral production and cell growth were measured every other day after HIV-1 IIIB infection at the MOI of 0.07. As shown in Fig. 2A, in the beginning of the culture from day 0 to day 4, cell growth was similar among CEM-SS cells, MazF-transduced CEM-SS cells, and GFP-transduced CEM-SS cells, as well as uninfected CEM-SS cells. CEM-SS cells harboring the *mazF* (ACA-less) gene grew at a normal rate throughout the time course of HIV-1 IIIB infection, whereas both GFP-transduced CEM-SS cells and the parental cell line showed aberrant growth rates due to HIV-1 infection in late cultures after day 8 (Fig. 2A). Indeed, a high level of p24 was detected in the GFP-transduced cell populations during the course of infection (Fig. 2B). In the case of MazF-transduced cells, however, levels of p24 were three orders of magnitude lower than those of GFP-transduced cells throughout the experiment (Fig. 2B). Notably, CD4 levels of MazF-transduced cells infected with HIV-1 IIIB were largely unaffected (Fig. 3B). Together with the fact that the HIV-1 IIIB infected cells harboring the *mazF* gene grew normally (Fig. 2A), these results suggest that HIV-1 IIIB gene expression in the HIV-1-LTR-regulated *mazF* (ACA-less)-transduced cells is effectively inhibited by blocking HIV-1 replication with little damage to cellular function.

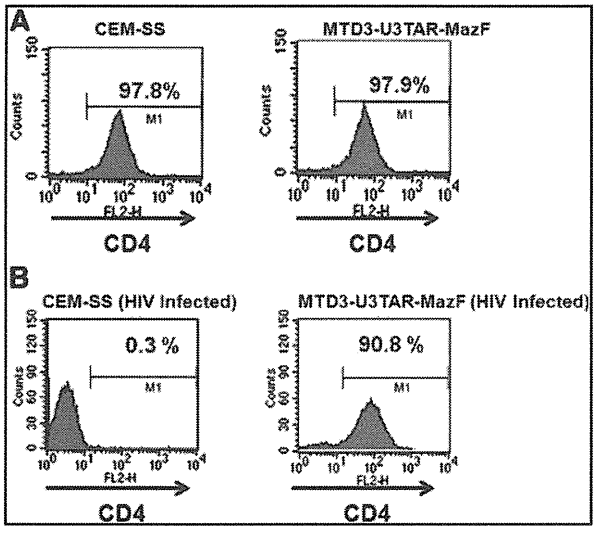

FIG. 3. CD4 levels in MazF-transduced cells. (**A**) Endogenous expression levels of CD4 were analyzed using PE-labeled anti-human CD4 antibody following flow cytometric analysis. (**B**) CEM-SS control cells and CEM-SS cells transduced with MTD3-U3TAR-MazF were infected with HIV-1 IIIB at an MOI of 0.007. After infection, the cells were maintained for 5 weeks and CD4 expression levels were analyzed using PE-labeled anti-human CD4 antibody following flow cytometric analysis.

Next, we examined if HIV-1 IIIB was integrated into the genome of MazF-transduced CEM-SS cells upon HIV-1 infection. Two different regions of the HIV-1 *gag* gene were amplified by PCR using genomic DNA 14 days after HIV-1 IIIB infection. As shown in Fig. 2C, both regions of the *gag* gene were detected in the genome of MazF-transduced CEM-SS cells, which were resistant to HIV-1 replication (lane 3). Similarly, HIV-1 DNA was detected in the genomes of CEM-SS cells (lane 2) and H9-IIIB cells (lane 4) (positive control H9 cells chronically infected with HIV-1 IIIB), whereas no bands were detected in noninfected cells (lane 1). We also established a CEM-SS cell line chronically infected with HIV-1 IIIB (CH-1). When this cell line was mixed with CEM-SS cells or MazF-transduced CEM-SS cells at a ratio of 10, 1, or 0.1%, CEM-SS cells were gradually infected with HIV-1 produced from CH-1 cells (Fig. 2D) and their cell growth was suppressed. Alternatively, MazF-transduced CEM-SS cells showed no growth inhibition (data not shown), indicating that HIV-1 replication was suppressed in MazF-transduced CEM-SS cells. As a result, the culture was eventually taken over by normally growing MazF-transduced CEM-SS cells over the slow-growing CH-1 cells. These data demonstrate that MazF-transduced cells are resistant to HIV-1 IIIB infection by blocking HIV-1 IIIB replication.

To investigate the *mazF* gene expression and subsequent effects more precisely, CEM-SS cells and CEM-SS cells transduced with MTD3-U3TAR-MazF were infected with the Tat-expressing retroviral vectors, M-LTR-Tat-ZG or H-LTR-Tat-ZG (Fig. 5A). Induction of the *mazF* gene in CEM-SS cells transduced with MTD3-U3TAR-MazF was monitored by real-time PCR, and the relative ratios were compared with mock infection (Fig. 5B). Infected cells were also subjected to

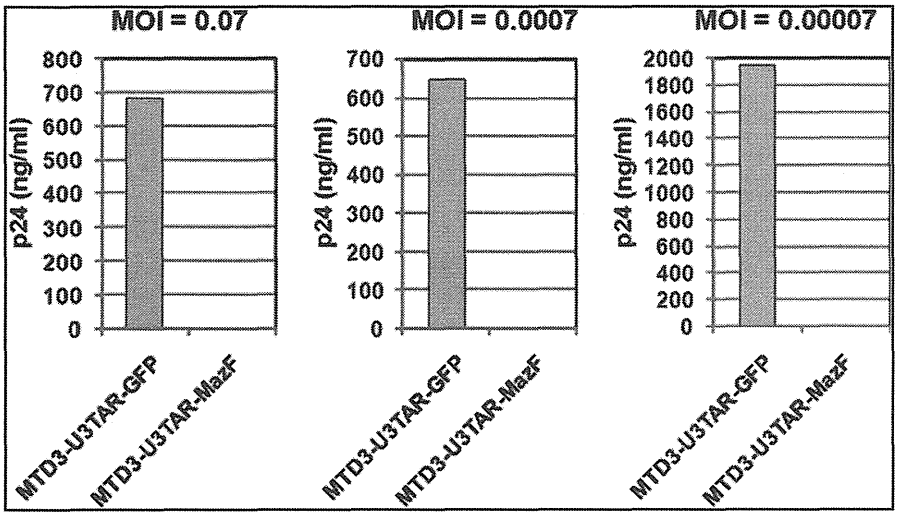

FIG. 4. HIV-1 IIIB infection using MazF-transduced CEM-SS cells at different MOIs. Polyclonal cell populations of CEM-SS resulting from gene transduction with retroviral vectors MTD3-U3TAR-MazF or MTD3-U3TAR-GFP were infected with HIV-1 IIIB at different MOIs (0.07, 0.0007, and 0.00007). Sixteen days after infection, HIV-1 p24 levels in the culture supernatant were estimated using the p24 ELISA kit (PerkinElmer). Given the cytopathic effect of HIV-1, the MTD3-U3TAR-GFP cell population showed delayed proliferation after HIV-1 infection in contrast to the MTD3-U3TAR-MazF population. The delay was more pronounced for the high-MOI group (0.07) than for the low-MOI group (0.00007) at later time points. On day 16 post infection, the accumulated cell number of the high-MOI group was threefold lower than that of the low-MOI group, so the difference in HIV-1 p24 levels between the two MOI groups (0.07 and 0.00007) reflects total cell numbers.

flow cytometry, and both Tat-positive (ZsGreen-positive) cells and dead cells (PI-positive) were monitored (Fig. 5B). As shown in Fig. 5B, strong induction of *mazF* expression was observed upon constitutive M-LTR-Tat-ZG vector transduction, and there was a significant decline in Tat-positive (ZsGreen-positive) cell population. On the other hand, *mazF* induction in HIV-LTR-driven Tat expression was lower, and the influence on cell death was also less than by MLV-LTR-driven Tat expression as observed in the PI-positive population. Although these experiments do not directly reflect HIV-1 replication, these data support the hypothesis that only low levels of MazF are expressed upon HIV-1 infection and MazF-positive cells can survive with HIV-1 provirus.

As the SIN-based retroviral vector contains the *mazF* gene in the normal orientation, the *mazF* gene is expressed from viral mRNA, resulting in the degradation of the viral RNA and thus significantly reducing the viral titer from this vector. On the other hand, when the MazF expression cassette is

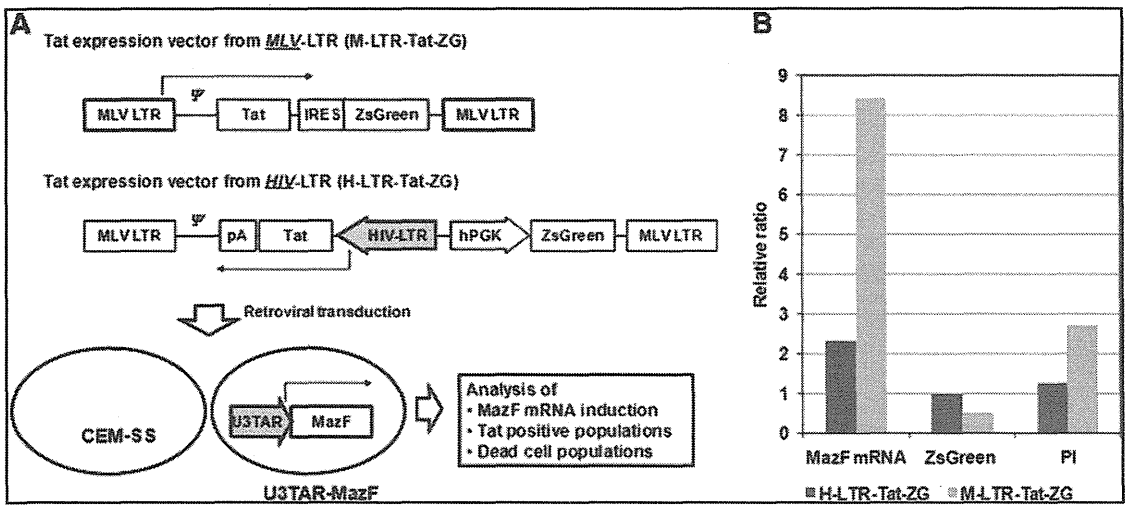

FIG. 5. Analysis of MazF induction upon Tat expression. (**A**) Outline of experimental procedure to analyze MazF induction upon Tat expression. (**B**) MazF mRNA levels were analyzed in MTD3-U3TAR-MazF transduced CEM-SS cells after Tat-expressing retroviral vector infection using real-time RT-PCR. The relative fold change is shown compared with that of mock infections. Tat-positive (ZsGreen-positive) cell populations and dead (PI-positive) cell populations in MTD3-U3TAR-MazF-transduced CEM-SS cells were analyzed by flow cytometry 2 days after different Tat retroviral vector transduction. The relative ratio is shown compared with that of CEM-SS cells.

inserted in the opposite direction from the retroviral genome, the viral titer increased and the gene transfer efficiency was improved more than 10 times (data not shown). To investigate the antiviral effect of the TAR-*mazF* system in the primary CD4+ T lymphocytes, the reversely orienting MT-MFR-PL2 vector was introduced into rhesus macaque primary CD4+ T cells from two individual monkeys (#14 and #15). The resulting *mazF*-containing cells were then infected with SIV/HIV-1 chimeric virus SHIV 89.6P. As the SHIV 89.6P harbors HIV-1-derived *env*, *rev*, *vpu*, and *tat* genes, the TAR-*mazF* system is expected to function when MazF-Tmac cells are infected with SHIV 89.6P. Indeed, efficient suppression of SHIV 89.6P replication was observed for both primary cell lines, #14 and #15 (Fig. 6A).

To evaluate further how well the retroviral *mazF* system is able to suppress viral RNA production, total cellular RNAs were extracted from MazF-Tmac cells to estimate quantitatively the amounts of SHIV RNA, as well as the mRNAs for ribosomal protein L13a (RPL13a, XM_001093017) and β-actin (NM_001033084), by real-time PCR. The relative ratios were normalized by using 18S rRNA (FJ436026), which is protected from MazF cleavage in ribosomes (Shimazu *et al.*, 2007). We obtained similar results in MazF-Tmac cells from both #14 and #15 primary cell lines. Representative results from MazF-Tmac cells from #14 are shown in Fig. 6B, where one can see that SHIV RNA was preferentially cleaved, whereas the cellular mRNAs were not affected. These results clearly demonstrate that MazF induction from the Tat system upon SHIV 89.6P infection leads to severe defect in maintaining SHIV 89.6P RNA but does not affect cellular mRNAs in SHIV-infected CD4+ T cells.

Discussion

This study demonstrates the distinct feasibility of RNase-based strategies for gene therapy. RNase-based strategies may be preferred over RNA-based strategies for HIV therapy, because RNases cleave HIV-RNA to cause permanent damage to HIV RNA function. Additionally, as RNases function as an enzymatic catalyst, they are required only at low concentrations in the cells to effectively block HIV proliferation. In the present study, the gene for MazF, an ACA-specific mRNA interferase, was engineered under the HIV-1 LTR promoter and inserted in the genome of the CD4+ T lymphoid cells so that MazF is expected to be produced only when the cells are infected with HIV-1 to produce the Tat protein. We demonstrated that *mazF*-Tmac cells indeed acquired resistance against SHIV replication, but cell growth was not inhibited after SHIV infection (data not shown), indicating that cellular mRNAs were not significantly affected. Notably, MazF was also able to function against the expression of SHIV proviral genome, because the production of SHIV in the culture supernatant was dramatically reduced.

Acquisition of HIV-1 resistance, and more remarkably the ability of MazF-transduced cells to suppress HIV-1 replication, may be explained as follows: Upon HIV-1 infection, Tat expression is first induced from the HIV-1 proviral genome. Tat then triggers the transcription of the *mazF* gene under the LTR promoter, as well as the full-length HIV proviral genome. The resulting induction of MazF expression leads to the cleavage of newly emerged HIV-1 mRNAs so that Tat protein synthesis is no longer sustainable. However, it is important to note that HIV-1 infection does not hamper cell growth and that the HIV-1 provirus genome is retained in the MazF-transduced cells. Therefore, the cellular level of Tat appears to be maintained at a very low level so that the level of MazF induction is also kept very low enough to cleave HIV-1 mRNAs, but not cellular mRNAs. Depending on the integration site and proviral copy number, there might be some MazF-transduced cells that were not resistant to HIV-1 replication. However, these cells could not survive due to HIV-1-induced cell death.

In mammals, virus infection is known to activate the interferon response to induce RNaseL, which mediates degradation of 28S and 18S ribosomal RNAs. This results in inhibition of protein synthesis as part of the host antiviral response (Silverman, 2003). An amphibian ribonuclease,

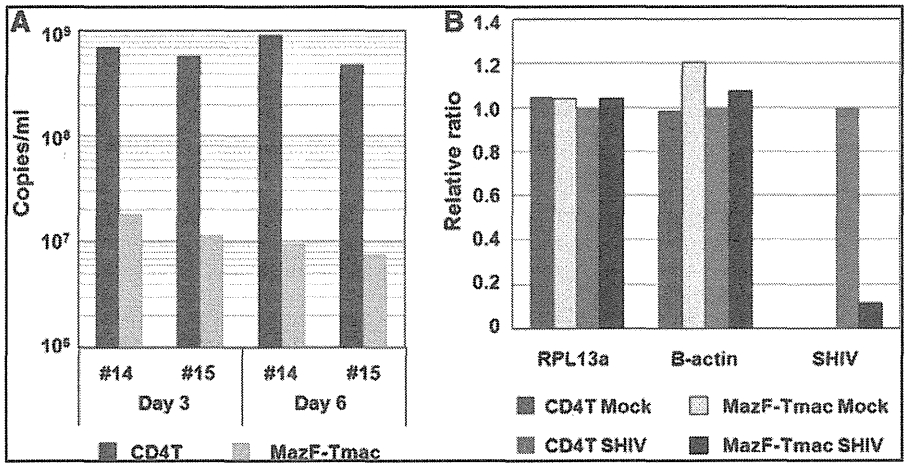

FIG. 6. Effect of MazF-induction into rhesus macaque primary CD4+ T cells on SHIV 89.6P replication. (**A**) Rhesus macaque primary CD4 T cells from two monkeys (#14 and #15) were activated and transduced with MT-MFR-PL2 vector. The MazF-transduced cells (MazF-Tmac cells) were re-activated with CD3/28 beads followed by infection with SHIV 89.6P. On days 3 and 6 post infection, culture supernatants were collected and evaluated for SHIV RNA copy by using the quantitative real-time PCR method. (**B**) Total cellular RNAs extracted from MazF-Tmac cells at 6 days post SHIV 89.6P infection were used to measure the amounts of SHIV RNA, as well as cellular housekeeping mRNAs, by using the quantitative real-time PCR method.

Onconase, is able to inhibit protein synthesis in mammalian cells and has been used as a protein drug. When it was added to the culture media of H9 cells persistently infected with HIV-1, HIV-1 replication was inhibited without blocking cell growth, as degradations of 18S and 28S rRNAs and cellular mRNAs were prevented (Saxena *et al.*, 1996). MazF induction in mammalian cells has shown to cause apoptotic cell death as a result of degradation of cellular mRNAs (Shimazu *et al.*, 2007). However, in the present study, MazF expression induced by HIV-1 Tat appears to be maintained at very low levels, just enough to cleave HIV-1 RNA but not cellular mRNAs, so that cells were able to grow normally. MazF expression may be autoregulated in the cell in such a way that when Tat-induced MazF eliminates invading HIV-1 RNA, Tat expression from the HIV-1 provirus is simultaneously stopped, resulting in simultaneous arrest of MazF production to recover normal cellular functions.

Targeting HIV RNA as a therapeutic strategy using antisense RNA (Levine *et al.*, 2006), ribonucleases (Agarwal *et al.*, 2006), and RNA interference (RNAi) technology (Morris and Rossi, 2004) has been attempted. However, the use of antisense RNA and RNAi technology has not been effective as an anti-HIV technology, as HIV can easily circumvent these RNA inhibitors by creating mutations at the target sequence regions (Lee and Rossi, 2004). On the other hand, the present strategy using MazF targets abundant ACA sequences in HIV-1 RNA (>240), so that it is not possible for HIV-1 to escape from MazF attack by mutations. Furthermore, because MazF has no homology to any mammalian ribonucleases, MazF mRNA interferase activity cannot be inhibited by ribonuclease inhibitors existing in mammalian cells.

In summary, the use of MazF appears to be a novel and highly effective tool for anti-HIV gene therapy. It is effectively able to suppress HIV-1 replication, preventing the emergence of mutated HIV-1. Importantly, MazF induction by invading HIV-1 shows little toxicity to host cells while it efficiently suppresses HIV-1 replication. Specific inhibition of HIV-1 replication by MazF without affecting cell growth is the key feature of MazF-based HIV-1 gene therapy. This may be the first step for RNase-based HIV-1 gene therapy with efficacy *in vitro*. The feasibility of the MazF-based *ex vivo* gene therapy may be verified using autologous CD4+ T lymphocytes from HIV-1 patients. To use our *mazF* vector system for gene therapy, its safety has to be critically evaluated and it should not have any negative impacts on T-cell function. For example, it needs to be shown that there is no alteration in the secretion of functionally important cytokines even though it was observed that MazF expression in HIV-infected CD4+ T cells does not inhibit cell growth. We are currently addressing this question.

Acknowledgments

The authors thank Dr. Keith A. Reimann of Harvard Medical School and Dr. Tomoyuki Miura of Kyoto University for providing the SHIV 89.6P. The authors also thank Dr. Koich Inoue of Takara Bio Inc. for his critical reading of the manuscript.

Author Disclosure Statement

No competing financial interests exist.

References

Agarwal, S., Nikolai, B., Yamaguchi, T., Lech, P., and Somia N.V. (2006). Construction and use of retroviral vectors encoding the toxic gene barnase. Mol. Ther. 14, 555–563.

Berkhout, B., Silverman, R.H., and Jeang, K.T. (1989). Tat transactivates the human immunodeficiency virus through a nascent RNA target. Cell 59, 273–282.

Kim, S., Ikeuchi, K., Byrn, R., Groopman, J., and Baltimore, D. (1989). Lack of a negative influence on viral growth by the nef gene of human immunodeficiency virus type 1. Proc. Natl. Acad. Sci. U.S.A. 86, 9544–9548.

Lee, J.T., Yu, S.S., Han, E., Kim, S., and Kim, S. (2004). Engineering the splice acceptor for improved gene expression and viral titer in an MLV-based retroviral vector. Gene Ther. 11, 94–99.

Lee, N.S., and Rossi, J.J. (2004). Control of HIV-1 replication by RNA interference. Virus Res. 102, 53–58.

Levine, B.L., Humeau, L.M., Boyer, J., MacGregor, R.R., Rebello, T., Lu, X., Binder, G.K., Slepushkin, V., Lemiale, F., Mascola, J.R., Bushman, F.D., Dropulic, B., and June, C.H. (2006). Gene transfer in humans using a conditionally replicating lentiviral vector. Proc. Natl. Acad. Sci, U.S.A. 103, 17372–17377.

Miyake, A., Ibuki, K., Enose, Y., Suzuki, H., Horiuchi, R., Motohara, M., Saito, N., Nakasone, T., Honda, M., Watanabe, T., Miura, T., and Hayami, M. (2006). Rapid dissemination of a pathogenic simian/human immunodeficiency virus to systemic organs and active replication in lymphoid tissues following intrarectal infection. J. Gen. Virol. 87, 1311–1320.

Morris, K.V., and Rossi, J.J. (2006). Lentivirus-mediated RNA interference therapy for human immunodeficiency virus type 1 infection. Hum. Gene Ther. 17, 479–486.

Nariya, H., and Inouye, M. (2008). MazF, an mRNA interferase, mediates programmed cell death during multicellular Myxococcus development. Cell 132, 55–66.

Reimann, K.A., Li, J.T., Voss, G., Lekutis, C., Tenner-Racz, K., Racz, P., Lin, W., Montefiori, D.C., Lee-Parritz, D.E., Lu, Y., Collman, R.G., Sodroski, J., and Letvin, N.L. (1996). An env gene derived from a primary human immunodeficiency virus type 1 isolate confers high in vivo replicative capacity to a chimeric simian/human immunodeficiency virus in rhesus monkeys. J. Virol. 70, 3198–3206.

Saxena, S.K., Gravell, M., Wu, Y.N., Mikulski, S.M., Shogen, K., Ardelt, W., and Youle, R.J. (1996). Inhibition of HIV-1 production and selective degradation of viral RNA by an amphibian ribonuclease. J. Biol. Chem. 271, 20783–20788.

Shimazu, T., Degenhardt, K., Nur-E-Kamal, A., Zhang, J., Yoshida, T., Zhang, Y., Mathew, R., White, E., and Inouye, M. (2007). NBK/BIK antagonizes MCL-1 and BCL-XL and activates BAK-mediated apoptosis in response to protein synthesis inhibition. Genes Dev. 21, 929–941.

Silverman, R.H. (2003). Implications for RNase L in prostate cancer biology. Biochemistry 42, 1805–1812.

Verzeletti, S., Bonini, C., Marktel, S., Nobili, N., Ciceri, F., Traversari, C., and Bordignon, C. (1998). Herpes simplex virus thymidine kinase gene transfer for controlled graft-versus-host disease and graft-versus-leukemia: clinical follow-up and improved new vectors. Hum. Gene Ther. 9, 2243–2251.

Yamaguchi, Y., and Inouye, M. (2009). mRNA interferases, sequence-specific endoribonucleases from the toxin-antitoxin systems. Prog. Mol. Biol. Transl. Sci. 85, 467–500.

Yu, S.F., von Rüden, T., Kantoff, P.W., Garber, C., Seiberg, M., Rüther, U., Anderson, W.F., Wagner, E.F., and Gilboa, E.

(1986). Self-inactivating retroviral vectors designed for transfer of whole genes into mammalian cells. Proc. Natl. Acad. Sci. U.S.A. 83, 3194–3198.

Yu, S.S., Han, E., Hong, Y., Lee, J.T., Kim, S., and Kim, S. (2003). Construction of a retroviral vector production system with the minimum possibility of a homologous recombination. Gene Ther. 10, 706–711.

Zhang, Y., Zhang, J., Hoeflich, K.P., Ikura, M., Qing, G., and Inouye, M. (2003). MazF cleaves cellular mRNAs specifically at ACA to block protein synthesis in *Escherichia coli*. Mol. Cell 12, 913–923.

Zhu, L., Zhang, Y., The, J.S., Zhang, J., Connell, N., Rubin, H., and Inouye, M. (2006). Characterization of mRNA interferases from Mycobacterium tuberculosis. J. Biol. Chem. 281, 18638–18643.

Zhu, L., Inoue, K., Yoshizumi, S., Kobayashi, H., Zhang, Y., Ouyang, M., Kato, F., Sugai, M., and Inouye, M. (2009). *Staphylococcus aureus* MazF specifically cleaves a pentad sequence, UACAU, which is unusually abundant in the mRNA for pathogenic adhesive factor SraP. J. Bacteriol. 191, 3248–3255.

Address correspondence to:
Dr. Ikunoshin Kato
Center for Cell and Gene Therapy
Takara Bio Inc.
Seta 3-4-1
Otsu, Shiga
520-2193, Japan

E-mail: ikukatiku@zeus.eonet.ne.jp

Dr. Masayori Inouye
Department of Biochemistry
Robert Wood Johnson Medical School
675 Hoes Lane
Piscataway, NJ 08854, USA

E-mail: inouye@umdnj.edu

Received for publication January 5, 2010;
accepted after revision July 22, 2010.

Published online: July 22, 2010.

Virology 421 (2011) 96–104

Contents lists available at SciVerse ScienceDirect

Virology

journal homepage: www.elsevier.com/locate/yviro

Analyses of mutations selected by passaging a chimeric flavivirus identify mutations that alter infectivity and reveal an interaction between the structural proteins and the nonstructural glycoprotein NS1

Evandro R. Winkelmann [a], Douglas G. Widman [b,d], Ryosuke Suzuki [a,e], Peter W. Mason [a,b,c,f,*]

[a] Department of Pathology, University of Texas Medical Branch, Galveston, TX 77555-0436, USA
[b] Department of Microbiology and Immunology, University of Texas Medical Branch, Galveston, TX 77555-0436, USA
[c] Sealy Center for Vaccine Development, University of Texas Medical Branch, Galveston, TX 77555-0436, USA
[d] Lineberger Comprehensive Cancer Center, University of North Carolina, Chapel Hill, NC 27599-7295, USA
[e] National Institute of Infectious Diseases, Shinjuku-ku, Tokyo 162-8640, Japan
[f] Microbial Molecular Biology, Novartis Vaccines and Diagnostics, Cambridge, MA, 02139, USA

ARTICLE INFO

Article history:
Received 6 May 2011
Returned to author for revision 6 June 2011
Accepted 8 September 2011
Available online 13 October 2011

Keywords:
Flavivirus
Single-cycle virus
Chimera
RepliVAX
Packaging

ABSTRACT

We previously described a single-cycle dengue vaccine (RepliVAX D2) engineered from a capsid (C) gene-deleted West Nile virus (WNV) expressing dengue virus serotype 2 (DENV2) prM/E genes in place of the corresponding WNV genes. That work demonstrated that adaptation of RepliVAX D2 to grow in WNV C-expressing cells resulted in acquisition of non-synonymous mutations in the DENV2 prM/E and WNV NS2A/NS3 genes. Here we demonstrate that the prM/E mutations increase the specific infectivity of chimeric virions and the NS2A/NS3 mutations independently enhance packaging. Studies with the NS2A mutant demonstrated that it was unable to produce a larger form of NS1 (NS1'), suggesting that the mutation had been selected to eliminate a ribosomal frame-shift "slippage site" in NS2A. Evaluation of a synonymous mutation at this slippage site confirmed that genomes that failed to make NS1' were packaged more efficiently than WT genomes supporting a role for NS1/NS1' in orchestrating virion assembly.

Introduction

Flaviviruses are single-stranded, positive-sense RNA viruses and have an 11-kb genome with a single open reading frame encoding three structural proteins (C, prM/M and E) and seven non-structural proteins (NS1, NS2A, NS2B, NS3, NS4A, NS4B and NS5). Flavivirus RNA replication occurs in the cell cytoplasm via a negative-strand RNA intermediate, ultimately leading to the accumulation of positive-strand RNAs. Several NS proteins have been implicated in genome replication. The NS2B/NS3 serine protease is required for proteolytic processing at multiple sites in the viral polyprotein. NS3 also possesses RNA triphosphatase and RNA helicase activities and NS5 contains methyltransferase and RNA-dependent RNA polymerase activities (Lindenbach et al., 2007). NS1 is a non-structural glycoprotein that is secreted from mammalian but not insect cells infected by flaviviruses (Mason, 1989), and is found at high concentrations in the blood of viremic dengue patients (Alcon et al., 2002; Libraty et al., 2002).

NS1 is found in the viral polyprotein immediately following the two structural proteins, prM/E. The coding regions of these proteins are separated by signal peptidase cleavage sites, and all three proteins acquire N-linked carbohydrates during their synthesis (Lindenbach et al., 2007). prM and E form heterodimers which eventually undergo a complicated maturation process that produces E dimers that cover the surface of the mature viral particle (Li et al., 2008; Yu et al., 2008). Early studies demonstrated that NS1 was slowly secreted from mammalian cells, and studies with trans-expressed prM/E/NS1 cassettes suggested a role for NS1 in virion morphogenesis (Fan and Mason, 1990; Konishi et al., 1991; Mason, 1989). However, work with NS1 mutants demonstrated that NS1 played an essential role in viral RNA replication (Muylaert et al., 1996; Muylaert et al., 1997).

The insect-vectored flaviviruses are responsible for considerable morbidity and mortality worldwide. The viruses exist on all continents of the world except Antarctica, and threaten much of the world's population. DENV infections are estimated to occur in up to 100 million individuals annually and over 2.5 billion people live in areas at risk for DENV infection. Vaccines are available for a number of flavivirus diseases, including YF and JE, but there are currently no vaccines available for dengue. Among the marketed vaccines, the YF vaccine, which consists of the live-attenuated strain YF-17D, has been widely recommended to travelers, and has been considered to be remarkably safe and efficacious. However, recent documentation

* Corresponding author at: Novartis Vaccines and Diagnostics, Inc., 45 Sidney Street, Cambridge, MA 02139, USA.
E-mail address: peter.mason@novartis.com (P.W. Mason).

0042-6822/$ – see front matter © 2011 Elsevier Inc. All rights reserved.
doi:10.1016/j.virol.2011.09.007

of disease in a tiny fraction of those vaccinated with YF-17D prompted reconsideration of its safety and as a result, the American Committee on Immunization Practices now recommends that the risk of infection with YFV be taken into account when vaccinating travelers from non-endemic regions (Staples et al., 2010). Nevertheless, YF-17D continues to be an important public health tool, and has undisputable benefit in populations at high risk of YFV infection. In the case of JE vaccines, a live-attenuated vaccine is widely used in China, but safety and manufacturing issues have restricted it from being used in other regions of the world (Halstead and Thomas, 2011). In these areas, the product of choice was an efficacious inactivated mouse-brain derived virus, but safety concerns prompted its removal from use. However, new products, including cell-culture derived inactivated vaccines and a chimeric live-attenuated product based on YFV 17D are now being marketed in developed economies (Halstead and Thomas, 2011).

Recently, we reported the development of single-cycle flaviviruses that can be used as safe and effective vaccines (Mason et al., 2006). This single-cycle technology has been used to produce a series of vaccine candidates (named RepliVAX), that encode genomes harboring a truncated C (trC) gene that prevents the RepliVAX genome from being packaged into infectious particles unless the C gene is supplied in *trans* (Ishikawa et al., 2008; Mason et al., 2006; Suzuki et al., 2009; Widman et al., 2008). RepliVAX can infect normal cells in vaccinated animals, and these infected cells release prM/E-containing sub-viral particles (SVPs) and NS1 that induce effective antiviral immune responses. However, RepliVAX cannot spread or cause disease in animals, thus making them safe live-attenuated vaccines. The most recent addition to the RepliVAX family is a chimeric RepliVAX that expresses the prM/E genes of DENV2 in place of the WNV structural genes, and this vaccine (RepliVAX D2) was able to control DENV2 disease in a mouse model for DENV2 infection (Suzuki et al., 2009).

During our development of RepliVAX D2, we discovered that the initial construct grew poorly in C-expressing cells, but that growth could be improved by extensive blind passage (facilitated by introduction of larger fragments of the C gene and passaging of packaging cells along with the single-cycle virus). Analyses of these blind-passaged variants demonstrated that their improved growth characteristics were associated with the acquisition of specific mutations in the coding regions for prM, E, NS2A and NS3. In the case of the mutations in prM and E, we used reverse genetics to show that a pair of mutations in M (amino acid 9: G->R and amino acid 13: E->V; referred to by convention as $M^{R9G,V13E}$) and a single mutation in E (E^{K120T}; numbering convention as shown for M) both operated individually to increase yield of RepliVAX D2 in culture, but the combination of the M and E mutations worked together to produce the greatest enhancement in viral growth (Suzuki et al., 2009). Further, we showed that the mutations in the NS2A ($NS2A^{S9F}$) and the NS3 genes of the WNV backbone ($NS3^{R516K}$) enhanced growth of a re-engineered RepliVAX D2, but did not appear to have an effect on genome replication *per se*, since they were unable to enhance replication of WNV replicons that did not contain DENV genes (Suzuki et al., 2009).

Here we report that the mutations we identified in the growth-adapted chimeric RepliVAX D2 constructs in the DENV2 prM and E region improve specific infectivity of flavivirus particles in a manner similar to that of a previously characterized heparan sulfate (HS)-binding mutation at a nearby position in E (E^{K126E}) (Lee et al., 2006). In addition, we demonstrate that the mutation in the WNV NS2A (which acts in concert with the WNV NS3 mutation) eliminates the production of an altered form of NS1 (NS1') that arises from ribosome slippage at a site found in WNV, but not DENV (Firth and Atkins, 2009; Melian et al., 2010). Finally, we demonstrate that the elimination of the production of NS1' by introduction of a synonymous mutation in this ribosomal slippage site improved encapsidation of particles without altering the amplification and translation of the genome, indicating a functional interaction between NS1/NS1' and the structural proteins of flaviviruses during encapsidation.

Results

Mutations in DENV prM/E increase growth and alter specific infectivity

To determine how growth-enhancing mutations in the DENV2 prM/E coding region of single-cycle chimeric flaviviruses expressing the prM/E genes of DENV2 and the NS genes of WNV function (Suzuki et al., 2009), we produced a series of packaging cell lines (see Fig. 1A) that encoded the low passage DENV2 New Guinea C (NGC) prM/E sequences [BHK(VEErep/WNVC*-DENV2prM/E/Pac)] used to make our first generation RepliVAX D2 as well as a cell line [BHK(VEErep/WNVC*-DENV2pr/$M^{R9G,V13E}$/E^{K120T}/Pac)] that encoded the DENV2 prM/E sequences selected when RepliVAX D2 was adapted to grow in cells expressing the C gene (Suzuki et al., 2009). These packaging cells, along with cell lines carrying packaging constructs expressing the WNV prM/E [BHK(VEErep/WNVC*-E/Pac)], the JEV prM/E [BHK (VEErep/WNVC*-JEVprM/E/Pac)], and a cell line [BHK(pVEErep/WNVC*-DENV2prM/E^{K126E}/Pac] expressing an E protein from a high-passage NGC strain of DENV that contains a DENV2 E mutation (E^{K126E}) previously associated with HS binding (Lee et al., 2006) (see Fig. 1A) were used to produce viral replicon particles (VRPs) containing a WNV replicon (C-hFLuc2A-NS1-5, see Fig. 3A). When these VRPs, which contained identical WNV-derived replicons transpackaged in the different coats provided by their packaging cell lines (Fig. 1A), were tested side-by-side for their specific infectivities in Vero cells (genome copies per IU; see Materials and methods), we discovered that the VRPs packaged in WNV or JEV prM/E proteins exhibited significantly better specific infectivities (500 to 2000 genome copies per IU) than particles packaged in any of the DENV2 coats (50,000 to 200,000 genome copies per IU; Fig. 1B). Among the DENV2-packaged VRPs, the VRPs coated with the prM/E proteins of a low-passage NGC strain [from BHK(VEErep/WNVC*-DENV2prM/E/Pac)] displayed the poorest infectivity (over 200,000 genome equivalents per IU), and the particles packaged in coats containing the previously identified HS-binding mutation at position 126 (Lee et al., 2006) [BHK(pVEErep/WNVC*-DENV2prM/E^{K126E}/Pac)] displayed a slightly better specific infectivity. Interestingly, the VRPs packaged in the cell lines encoding the DENV2 prM/E genes selected in our RepliVAX D2 passaging studies (Suzuki et al., 2009) [BHK(VEErep/WNVC*-DENV2pr/$M^{R9G,V13E}$/E^{K120T}/Pac)] displayed a significantly better specific infectivity than the particles packaged in the WT DENV2-packaged VRPs, which contained the same low-passage DENV2 genes used to initiate the passaging studies we performed with RepliVAX D2 (Suzuki et al., 2009) (Fig. 1B). Taken together, these data demonstrate that the previously reported low-specific infectivity of DENV particles (van der Schaar et al., 2007) is due to the properties of the virion surface proteins and that changes in specific infectivity in cell culture can be facilitated by addition of positively charged residues in M and E that presumably function by facilitating productive binding of negatively charged glycosaminoglycans (GAGs) such as HS that are ubiquitously expressed on cells in culture and aid in infection as previously demonstrated for DENV2 (Lee et al., 2006). However, we cannot rule out the possibility that the mutations in prM/E could also have a role in the maturation of the structural proteins needed for flavivirus morphogenesis, especially in light of recent work showing that extracellular DENV particles contain a mixture of mature (lacking prM) and immature particles (Junjhon et al., 2010) which likely contribute to their poor specific infectivity.

NS2A and NS3 mutations previously selected in DENV2/WNV chimeras improve VRP growth when packaged in DENV2 envelopes

During propagation of a derivative of RepliVAX D2 containing the prM/E mutations described above (Suzuki et al., 2009), two mutations were selected in the WNV nonstructural protein-encoding regions that improved the growth of these chimeric viruses. To help learn how these mutations exerted their effects, we introduced

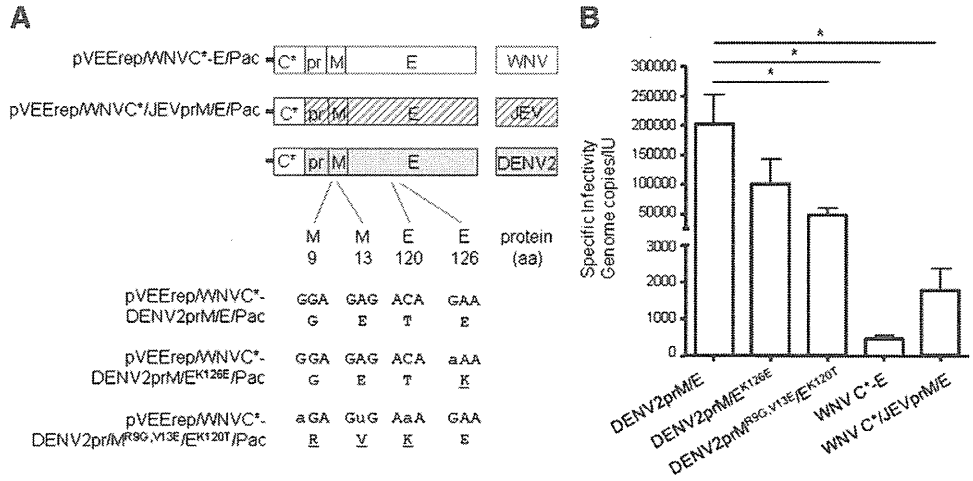

Fig. 1. Effect of flavivirus M/E proteins on the specific infectivity of trans-encapsidated WNV replicon genomes. (A) Schematic representation of the packaging cell constructs. All constructs contained a form of the WNV C protein (C*) engineered to contain synonymous mutations in the start of the genome to prevent generation of homologous recombinants with the replicons, as well as complete prM/E cassettes from the indicated viruses (see Materials and methods); "aa" indicates the position of the affected codon within the individual protein-coding regions. (B). Specific infectivities of VRPs created by packaging a WNV-derived replicon [pWNR C-hFLuc2A NS1-5-encoding hFLuc (see Materials and methods and Fig. 3A)]. Data displayed indicate the particle number (determined by genome quantification using sqPCR) divided by the measured infectivity on Vero cells (see Materials and methods). Error bars indicate the standard deviation between specific infectivity determinations established from two measurements of RNA concentration from the linear range of the sqPCR standard curve. "*" denotes significance as measured by one-way ANOVA with Bonferroni post-test ($p<0.05$).

them into RepliVAX WN (as single or double mutations; Fig. 2A), and tested how these mutations affected the growth of this non-chimeric single-cycle virus in a WNV C-expressing cell line [BHK(VEErep/Pac-Ubi-C*)]. Fig. 2B shows growth curves for the WT and mutated RepliVAX WN that were created by averaging values from 3 independent experiments. These growth curves demonstrate that the mutations selected in the context of the chimeric RepliVAX D2 were unable to produce a detectable improvement in growth of the non-chimeric RepliVAX WN.

To further evaluate the interactions between WNV NS2A and NS3 mutations and the DENV2 prM/E cassettes, NS2A^{S9F} and NS3^{R516K} were introduced as single- or double-mutations into a WNV replicon encoding a humanized form of the firefly luciferase (hFLuc) reporter gene (Fig. 3A). Comparison of the ability of VRPs containing these replicons to grow in a subset of the packaging cells described in Fig. 1 demonstrated that each of the non-structural protein mutations enhanced growth in all three of the DENV2 packaging cell lines (Figs. 3B, C and D). In addition, the two mutations displayed an additive/synergistic effect on transpackaging within DENV2 envelopes (Figs. 3B, C and D). However, neither of these mutations (independently or together) produced a detectable improvement in the growth of this WNV-derived replicon when replicons carrying these mutations were propagated in packaging cells expressing the WNV envelope protein cassette (Fig. 3E).

NS2A^{S9F} mutation alters the production of a higher molecular weight form of NS1

The recent observation that the NS2A gene of encephalitic flaviviruses contains a frame-shift motif (Firth and Atkins, 2009) that permits the production of an altered form of NS1 [known as NS1'; (Melian et al., 2010)] identified over 20 years ago in cells infected with JEV (Mason, 1989) prompted us to further examine our NS2A^{S9F} mutation. Interestingly, this mutation disrupts the canonical UUUU portion of the ribosome slip site that produces NS1' (CCCUUUU->CCCUUcU; Fig. 4A). To confirm that this mutation prevented the synthesis of NS1', we conducted Western blot analyses, that clearly demonstrate that this mutation results in the loss of NS1' (Fig. 4B).

Mutation of the ribosome slip site in NS2A enhances packaging of WN replicons in DENV2 coats and eliminates production of NS1'

To demonstrate that the growth enhancing properties of the NS2A^{S9F} mutation resulted through the abrogation of NS1' production, we engineered two silent mutations (CCCUUUU->CCC cUUc) in this region of NS2A (producing a construct designated NS2A^{F9F}) that disrupted the ribosome slip site (Fig. 5A). WNV replicons bearing this mutation alone, or in the presence of the NS3 mutation, displayed a significant enhancement of growth compared to the WT replicon genome when they were grown in cell lines providing DENV2 coats (Figs. 5B, C and D). Furthermore, Fig. 5E shows that the NS2A^{F9F} mutation, alone, or in concert with the NS3^{R516K} mutation produced a significant improvement in packaging in a WNV coat at several time points. As expected from the intentional disruption of the slippage site, cells infected with replicons expressing the NS2A^{F9F} mutation alone, or in the presence of the NS3^{R516K} mutation did not produce any detectable NS1' (Fig. 5F). To further understand the interaction between the NS2A^{F9F}and NS3^{R516K} mutations and DENV coats, we investigated the specific infectivity of C-hFLuc2A-NS1-5 and C-hFLuc2A-NS1-5 NS2A^{F9F} NS3^{R516K} VRPs produced in the WNVC*-DENV2pr/M^{R9G,V13E}/E^{K120T} and the WNVC*-E cell lines harvested from the 72 hpi time point in the study shown in Figs. 5D and E. These studies showed improved infectivity for the DENV-packaged VRPs that carried the NS2A frame-shift and NS3 mutations relative to the WT genomes, but no difference in the infectivity of the WNV-packaged genomes containing these mutations (Figs. S2A and B), suggesting that the C-hFLuc2A-NS1-5 NS2A^{F9F} NS3^{R516K} were more efficiently assembled into infectious DENV particles. Furthermore, Western blot analyses of the E protein content of these same VRP preparations showed a similar level of incorporation of WNV E into VRPs produced with either mutant or WT NS genes, but a more efficient incorporation of the DENV E into particles carrying the mutant NS genes, consistent with the hypothesis that the NS2A frame-shift and NS3 mutations produced higher infectious yields by increasing efficiency of assembly of infectious particles with DENV coats.

To further evaluate the role of these mutations in virion packaging in WNV coats, we utilized an additional, more sensitive assay consisting of calculating the size of infectious foci formed by VRPs carrying WT and mutant replicons on BHK(VEErep/WNVC*-E/Pac) cells.

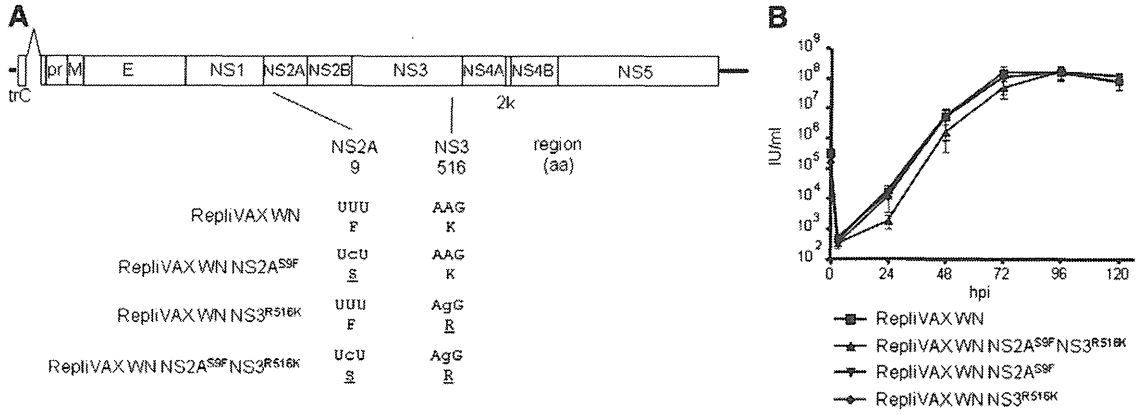

Fig. 2. NS2A^{S9F} and NS3^{R516K} mutations do not significantly improve the growth of RepliVAX derivatives carrying the WNV prM/E genes. (A) Schematic representation of derivatives of RepliVAX WN carrying mutations in NS2A and NS3; "aa" indicates the position of the affected codon within the individual protein-coding regions. (B) Growth curves of the RepliVAX WN constructs shown in Fig. 2A on BHK(VEErep/Pac-Ubi-C*) which express the WNV C protein. Cells were infected at an MOI of 0.01, and media were harvested, and titered at the indicated time points as described in the Materials and methods. The first time point (0 hpi) indicates the initial dose used to infect the cells. Values represent averages of three individual experiments. Error bars indicate standard deviation.

Fig. 6 shows the results of these assays, which support the data in Fig. 5E, by showing that all three VRPs tested in these assays tended to produce larger foci on cells expressing the WNV structural proteins.

NS1 is required for flavivirus genome replication, and mutations in NS1 have been shown to alter genome replication in cells in culture (see Introduction). To determine if the effect of NS1' abrogation was producing the enhanced growth/spread phenotype in packaging cell lines, we infected WT BHK cells with VRPs harboring various replicons and used the short-lived hFLuc reporter gene (Thompson et al., 1991) to quantify the levels of their genome replication and polyprotein translation. These studies, shown in Fig. 7, showed that neither the NS2A^{F9F}, NS3^{R516K}, nor the combined NS2A^{F9F}/NS3^{R516K} mutations significantly altered the levels of replicon amplification at 24 h post infection.

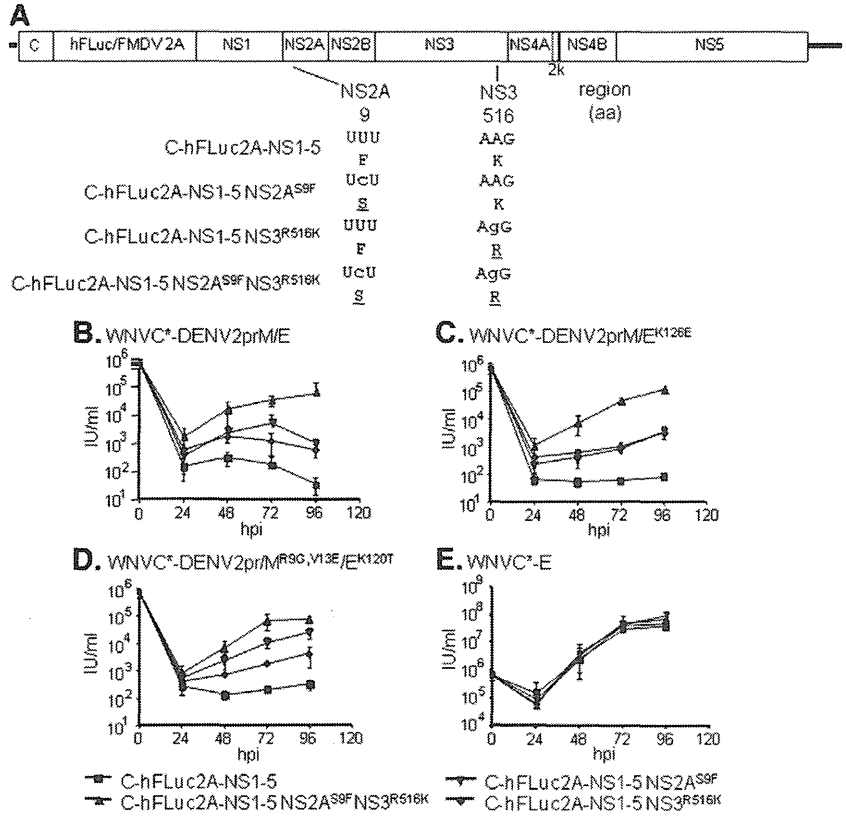

Fig. 3. NS2A^{S9F} and NS3^{R516K} improve growth of WNV VRPs when transpackaged in DENV coats. (A) Schematic representation of derivatives of WNV replicons carrying mutations in NS2A and NS3; "aa" indicates the position of the affected codon within the individual protein-coding regions. (B–E) Growth curves of VRPs harboring the genomes shown in Fig. 3A on BHK cell lines encoding the indicated packaging constructs. Cell monolayers were infected at an MOI of 0.05 with the indicated VRPs, and media were harvested and titered at the indicated time points as described in the Materials and methods. The first time point (0 hpi) indicates the initial dose used to infect the cells. Values represent averages of two individual experiments. Error bars indicate standard deviation.

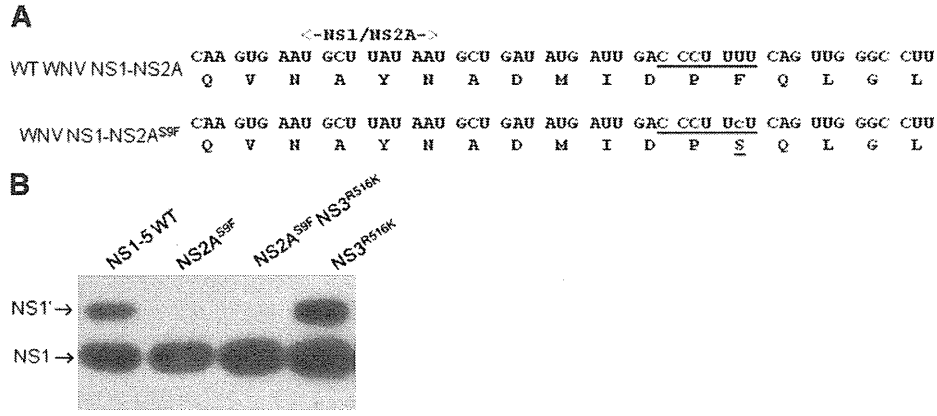

Fig. 4. Effect of NS2A^{S9F} mutation on synthesis of NS1'. (A) Alignment of RNA and amino acid sequences at the NS1/NS2A junction region of WNV showing the ribosomal frame-shift site (underlined) and its disruption by the NS2A^{S9F} mutation. (B) Western blot showing that cells infected with replicons encoding the NS2A^{S9F} mutation fail to produce NS1'. Cells infected with particles encoding C-hFLuc2A-NS1-5 replicon (labeled NS1-5 WT) and its derivatives (see Fig. 3A; labeled in this panel by mutation only) were lysed, blotted, and immunostained as described in the Materials and methods.

Discussion

Flaviviruses display a broad host- and cell-specificity which suggests that these viruses can use a variety of cell surface receptors. Multiple molecules have been identified that can serve as receptors, but the most clearly documented example of a cell-surface component that can be utilized as a receptor is the GAG, HS. Although the role of HS in natural infections by RNA viruses remains unclear, flaviviruses that are adapted to grow in cell culture or in specific animal models can acquire the ability to bind to HS through the acquisition of mutations on the E protein that produce positively charged patches that efficiently bind negatively charged GAGs (Anez et al., 2009; Kroschewski et al., 2003; Lee et al., 2004; Lee and Lobigs, 2000; Lee and Lobigs, 2002; Lee et al., 2006; Mandl et al., 2000). In the current studies we used a transpackaging system to demonstrate that the DENV2 M/E protein mutations found in our previously reported cell-adapted dengue chimera (Suzuki et al., 2009) improve the specific infectivity of transpackaged particles, explaining the selection of

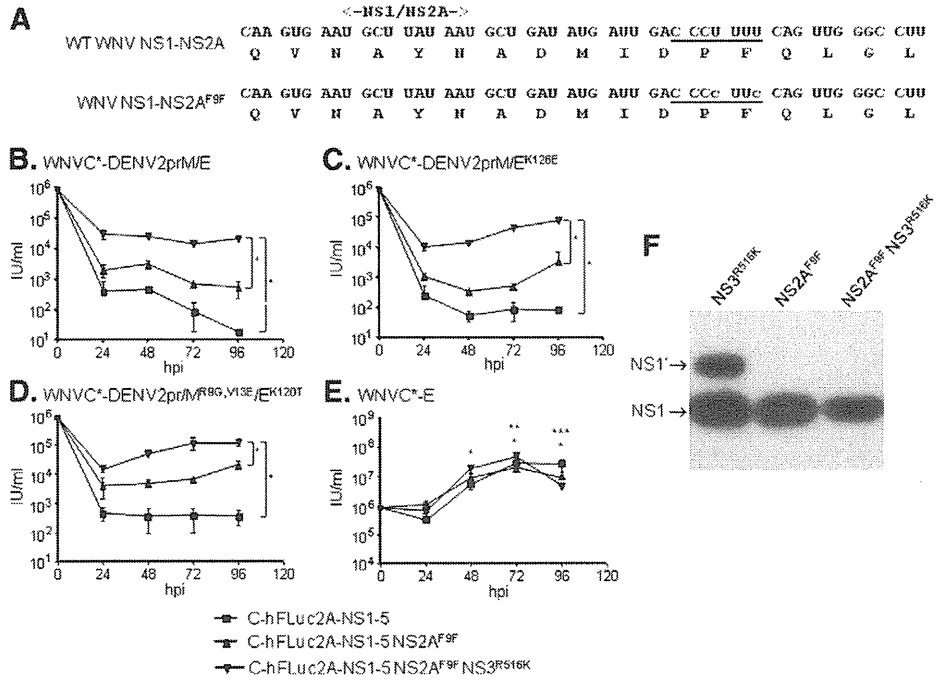

Fig. 5. Demonstration that ablation of ribosomal frame-shifting in NS2A enhances trans-encapsidation of WNV replicons and eliminates production of NS1'. (A) Alignment of RNA and amino acid sequences at the NS1/NS2A junction region of WNV showing the ribosomal frame-shift site (underlined) and its disruption by silent mutations. (B–E) Growth curves of VRPs harboring the WT replicon genomes, or genomes encoding the NS2A^{F9F} or NS2A^{F9F}NS3^{R516K} mutations on BHK cell lines encoding the indicated packaging constructs. Cell monolayers were infected at an MOI of 0.05 with the indicated VRPs, and media were harvested and titered at the indicated time points as described in the Materials and methods. The first time point (0 hpi) indicates the initial dose used to infect the cells. Values represent averages of two individual experiments. Error bars indicate standard deviation and "*" denotes significance as measured by two-way ANOVA with Bonferroni post-test ($p<0.05$) for 24–96 h timepoints (B and C) and 48–72 h timepoints (D). The same test showed significant differences in Fig. 5E; in this case: "*" denotes significance ($p<0.05$) for C-hFLuc2A-NS1-5 vs C-hFLuc2A-NS1-5NS2A^{F9F}NS3^{R516K}; "**" denotes significance ($p<0.05$) for C-hFLuc2A-NS1-5 NS2A^{F9F} vs C-hFLuc2A-NS1-5NS2A^{F9F}NS3^{R516K}; and "***" denotes significance ($p<0.05$) for C-hFLuc2A-NS1-5 vs C-hFLuc2A-NS1-5 NS2A^{F9F} at indicated timepoints. (F) Western blot showing that cells infected with VRPs containing the NS2A^{F9F} mutation fail to produce NS1'. Cells infected with particles encoding C-hFLuc2A-NS1-5 replicons encoding NS3^{R516K}, NS2A^{F9F}, or NS2A^{F9F} NS3^{R516K} mutations were lysed, blotted, and immunostained as described in the Materials and methods.

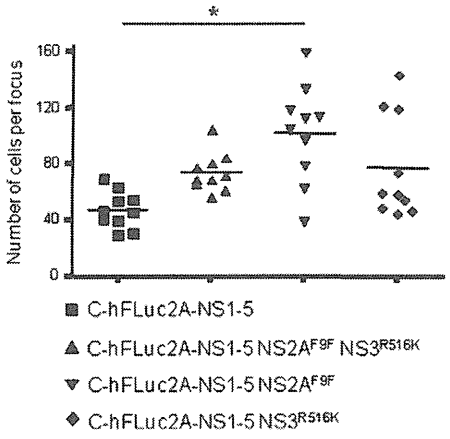

Fig. 6. Comparison of foci sizes of VRPs harboring the WT replicon genome, or genomes encoding the NS2A^{F9F}, NS2A^{F9F}NS3^{R516K} or NS3^{R516K} mutations on BHK(VEErep/WNVC*-E/Pac) cells expressing the WNV C-prM-E proteins. Cell monolayers were infected with serial dilutions of the VRPs, overlaid with semisolid medium, fixed, and immunostained with anti-NS1 antibody 48 h after incubation at 37 °C as described in the Materials and methods. The graph represents the counts of cells from 10 individual foci per VRP tested. The line represents the average of the 10 foci values for each group and "*" denotes significance as measured by one-way ANOVA with Bonferroni post-test ($p<0.001$).

these mutations during the adaptation of our dengue chimera to grow in cell culture. Furthermore, by comparing the specific infectivity of these preparations to those encoding envelopes of two encephalitic flaviviruses, we clearly demonstrated the poorer specific infectivity of particles encapsidated in DENV envelope proteins, consistent with work of Kuhn and co-workers documenting the poor specific infectivity of DENV2 virions (van der Schaar et al., 2007). Interaction among the proteins of positive-strand RNA viruses is one of the hallmarks of these viruses. Among the flaviviruses, numerous examples of such interactions exist within the structural proteins or within the well-defined non-structural protein complexes. Analyses of viable chimeras created from different species within the Flavivirus genus have revealed additional interactions. Several of these have documented interactions between components known to be involved in genome replication and the structural components of the virion. Among these, there has been a documented interaction of NS1 with the viral replicase via an interaction with NS4A (Lindenbach and

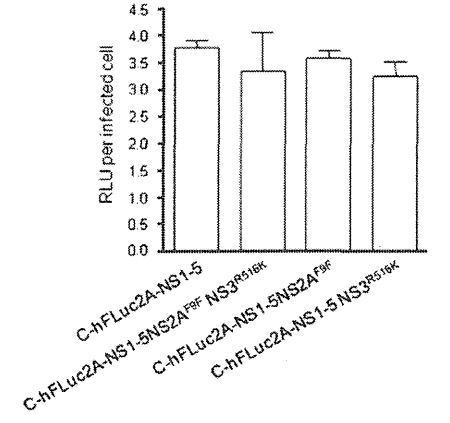

Fig. 7. Replication of VRPs harboring the WT replicon genome, or genomes encoding the NS2A^{F9F}, NS2A^{F9F}NS3^{R516K} or NS3^{R516K} mutations on BHK cells. Cells were cultured in 96-well plates, infected with VRPs and incubated for 24 h, when the relative luciferase units (RLU) were measured and then standardized to the number of VRP-infected cells obtained by immunostaining wells infected in a parallel plate (see Materials and methods). Data for each sample are averages of triplicate values with error bars showing standard deviations.

Rice, 1999). In a previous report we demonstrated that adaptation of a DENV/WNV single-cycle chimeric flavivirus to grow to higher titers in a specifically designed packaging cell line resulted in the selection of mutations in NS2A and NS3. Here we definitively demonstrate that these mutations exert their growth-enhancing effect by interaction with the structural proteins, and that this growth enhancing effect is more pronounced in the context of DENV2 structural proteins. These data explain how these adaptations arose in response to the unnatural chimerization. In the case of the mutation in NS3, we were unable to define the mechanism by which this mutation was exerting its phenotype, but the ability of this mutation which lies within the helicase domain of NS3 to improve packaging of the viral genome supports previous evidence showing that changes in the helicase domain can alter encapsidation (Patkar and Kuhn, 2008).

In the case of our NS2A mutation, which was found at codon 9 of the NS2A gene, we clearly demonstrate that this mutation functions through alteration of a recently documented ribosomal frame shift that produces an altered form of the NS1 protein (NS1') that is a characteristic of members of the JEV/WNV serocomplex of the flavivirus genus (Firth and Atkins, 2009; Mason, 1989; Melian et al., 2010). This interesting effect was evaluated by trans-complementation of genomes carrying the cell-adapted, non-synonymous mutation in NS2A which ablated the ribosome slippage site. These studies showed that this non-synonymous change increased transpackaging by prM/E proteins, and simultaneously eliminated the production of NS1'. The specific role of the frame shift in these phenotypes was confirmed by studies which demonstrated that synonymous mutations in this frame-shift site produced the same VRP growth-enhancing phenotype and ablation of NS1' production found in the non-synonymous mutation selected in our previous blind-passaging studies. Careful analyses of replicons harboring this mutation document that its effect on genome packaging, which was additive with the NS3 mutation, could be observed when packaging was evaluated in cells providing WNV or DENV2 prM/E coats. However, the growth-enhancing phenotype was more dramatic with the DENV2 prM/E coats, consistent with the hypothesis that these lower-specific infectivity coats provided a more significant selective pressure, allowing these mutations to arise in the chimeric background used for the initial passaging studies; the selection of these mutations is also consistent with preliminary studies showing that the combination of the NS2A frame-shift and NS3 point mutations into a replicon improve VRP yield from DENV E-producing cell lines by improving the specific infectivity of the resulting particles. Since the NS1 gene has been shown to serve a critical function in flavivirus genome replication we conducted studies to determine if ablation of NS1' by alteration of the slippage site could influence genome replication. These studies showed that abrogation of NS1' had no effect on genome replication, indicating that the mechanism by which NS1' alters particle packaging is due to an effect on virion assembly/release.

Our data demonstrating that the NS1' protein alters genome packaging expands the activities ascribed to the multifunctional NS1 protein. Although we have been unable to precisely determine how the larger form of the NS1 protein interferes with transpackaging of genomes into infectious particles, these findings are consistent with the slow egress of NS1 through the endoplasmatic reticulum (ER) of infected mammalian cells (Mason, 1989), the regulation of its localization to several compartments (Youn et al., 2010), the documented role of NS1 in genome replication (Muylaert et al., 1996; Muylaert et al., 1997), and interactions with NS4A (Lindenbach and Rice, 1999), all of which indicate that NS1 likely serves as a bridge between RNA synthesis and structural protein assembly. The finding that the extended form of NS1 has an inhibitory effect on virion packaging *in vitro* support this role. However, by themselves, these results are somewhat surprising. The fact that the effect on packaging was less pronounced in the presence of high-specific infectivity encephalitic flavivirus prM/E proteins is consistent with the fact that NS1' has

not been observed in other flaviviruses (see above). Interestingly, work by Khromykh and co-workers showed that abrogation of NS1' in a low-virulence isolate of WNV (Kunjin virus) reduced neurovirulence in mice (Melian et al., 2010). Although these studies did not document an effect of NS1' ablation on viral growth, they clearly showed an interesting effect of the NS1' protein *in vivo* but were unable to demonstrate any effect of the frame-shift ablation on growth of a mutant Kunjin virus *in vitro* in mammalian or insect cells (Melian et al., 2010). The inability to observe differences in growth of Kunjin viruses with or without the frame-shift mutation is consistent with our studies showing that productive growth of a single-cycle WNV (namely RepliVAX WN) in a complementing cell line was not improved by the introduction of this frame-shift mutation. Finally, although the influence of the frame shift on Kunjin virus neurovirulence may not provide an evolutionary advantage *per se*, the association of the frame-shift slippage site with the encephalitic flaviviruses likely reflects a selective biological advantage, which could be related to acquisition of additional functions by the larger form of NS1.

Materials and methods

Cells

BHK cells were maintained at 37 °C in minimal essential medium (MEM) supplemented with 10% fetal bovine serum (FBS) and antibiotics. Vero cells were maintained at 37 °C in MEM containing 6% FBS and antibiotics. BHK(VEErep/Pac-Ubi-C*) expressing the WNV C protein (Widman et al., 2008), BHK(VEErep/WNVC*-E/Pac) cells expressing the WNV C-prM-E proteins (Fayzulin et al., 2006), BHK(VEErep/WNC*-JEVprM-E/Pac) cells expressing the WNV C and JEV prM-E (Ishikawa et al., 2008), BHK(VEErep/WNVC*-DENV2prM/E/Pac) cells expressing the WNV C and the DENV2 NGC (low passage) prM/E (generated as described below), BHK(VEErep/WNVC*-DENV2prM/E^{K126E}/Pac) cells expressing the WNV C and a HS-binding E derived from a high-passage DENV2 NGC (generated as described below), and BHK(VEErep/WNVC*-DENV2pr/$M^{R9G,V13E}$/E^{K120T}/Pac) cells expressing the WNV C and the DENV2 prM/E mutations selected in RepliVAX D2 (generated as described below) were propagated at 37 °C in Dulbecco's MEM supplemented with 10% FBS and 10 μg/ml puromycin as previously described (Fayzulin et al., 2006).

Plasmid construction

The plasmid pWNR C-hFLuc2A NS1-5 encoding a WNV replicon expressing a hFLuc reporter gene has been previously described (Gilfoy et al., 2009). This was used to construct the various mutant WNV replicon plasmids with specific mutations in NS2A (pWNR C-hFLuc2A NS1-5 $NS2A^{S9F}$), NS3 (pWNR C-hFLuc2A CNS1-5 $NS3^{R516K}$), NS2A and NS3 (pWNR C-hFLuc2A NS1-5 $NS2A^{S9F}$/$NS3^{R516K}$), as well as a silent mutation in NS2A (pWNR C-hFLuc2A NS1-5 $NS2A^{F9F}$) using standard techniques (Higuchi et al., 1988).

The plasmid encoding the RepliVAX WN replicon [pRepliVAX WN (Widman et al., 2008); previously referred to as pRepliVAX WN.2 SP] was modified using standard techniques to produce a series of mutant RepliVAX WN plasmids with specific mutations in NS2A (pRepliVAX WN $NS2A^{S9F}$), NS3 (pRepliVAX WN $NS3^{R516K}$), and NS2A and NS3 (pRepliVAX WN $NS2A^{S9F}$/$NS3^{R516K}$) using standard techniques (Higuchi et al., 1988).

Plasmid pVEErep/WNVC*-E/Pac which encodes a Venezuelan equine encephalitis virus replicon (VEErep) capable of persisting in cells in the presence of puromycin and expressing the WNV structural proteins (C-prM-E) needed to package subgenomic replicons (Fayzulin et al., 2006) was used to construct a series of plasmids encoding a low-passage DENV2 NGC (Fonseca, 1994) prM/E cassette (pVEErep/WNVC*-DENV2prM/E/Pac), a high-passage DENV2 NGC (Fonseca, 1994) prM/E cassette (pVEErep/WNVC*-DENV2prM/E^{K126E}/Pac), or the prM/E cassette found in cell-adapted RepliVAX D2 (Suzuki et al., 2009) (pVEErep/WNVC*-DENV2pr/$M^{R9G,V13E}$/E^{K120T}/Pac). Sequences of all constructs are available from the authors upon request.

Production of packaging cell lines

Cell lines harboring replicons from the VEErep plasmids were created by a slight modification of the previously described procedures (Fayzulin et al., 2006). Briefly, the plasmid DNAs were linearized by using the MluI restriction enzyme, and the resulting template DNAs were *in vitro*-transcribed using MegaScript SP6 synthesis kit (Ambion) in the presence of 7mG(ppp)G cap analog (New England Biolabs). The yield and integrity of transcripts were determined by using non-denaturing gel electrophoresis, aliquots of transcription reactions were transfected into BHK cells using Lipofectin (Invitrogen), VEErep-harboring cell lines were selected in the presence of puromycin, and clones displaying high-level expression of these replicons were isolated and propagated using standard techniques.

Production of VRPs and RepliVAX WN derivatives

WNV replicon RNAs encoding the hFLuc gene (WNR C-hFLuc2A NS1-5 and derivatives) or the WNV prM/E cassette (RepliVAX WN and derivatives) were generated by using MegaScript T7 synthesis kit (Ambion) and 7mG(ppp)G cap analog (New England Biolabs) from SwaI-linearized templates created from the relevant plasmid DNAs using standard methods. Following analysis for yield and integrity as described above, aliquots of transcription reactions were electroporated into packaging cell lines (expressing C, prM, and E constructs in the case of the hFLuc-expressing replicon constructs or C only in the case of RepliVAX constructs) and then collected as previously described (Fayzulin et al., 2006).

VRP and RepliVAX titrations

VRPs and RepliVAX WN derivatives were titrated on Vero cells as previously described (Fayzulin et al., 2006). Yields are reported as infectious units per milliliter (IU/ml).

VRP and RepliVAX growth curves

To compare growth properties of the various WNV replicons in cell lines encoding various prM/E packaging constructs, VRPs derived from electroporations were used to infect these BHK packaging cells at a multiplicity of infection (MOI) of 0.05 for 2 h, the monolayers were washed 3 times (5 min each) with MEM supplemented with 1% FBS, 10 mM HEPES, and antibiotics, and the cultures were placed at 37 °C. Media were removed and replaced with fresh media at the indicated time points and stored at −80 °C for subsequent titration as described above.

Growth curves from RepliVAX WN and derivatives were prepared by infecting BHK(VEErep/Pac-Ubi-C*) cells at an MOI of 0.01 using the same procedure as described above.

Specific infectivity studies

Genome copy numbers and infectivity of VRPs produced by electroporation (see above) were determined based on semiquantitative PCR and Vero cell titration data. Briefly, VRP preparations were diluted to give titers of 1000 IU/ml, and one portion was titered on Vero cells as described above, while RNA was isolated from a second portion using the QIAamp Viral RNA kit (QIAGEN) following the manufacturer's protocol. The viral RNA concentration in this sample was determined by using a semiquantitative PCR (sqPCR) assay in which serial 2-fold dilutions of RNA from each sample were used for reverse transcription (RT) carried out with an ImProm II RT kit (Promega)

with random hexamers followed by amplification of a 100 bp PCR product using previously described WNV NS5-specific primers (Bourne et al., 2007). The PCR conditions included an initial cycle of 5 min at 95 °C, 30 cycles of 30 s at 95 °C, 30 s at 53 °C and 30 s at 72 °C, followed by 5 min at 72 °C. Following amplification, the PCR products were resolved by electrophoresis on 2% agarose gels containing 200 ng/ml of ethidium bromide, and images of the gels were acquired with a CCD camera using a FluorChem 8900 Chemiluminescence Gel Imager (Alpha Innotech) and band intensities were quantified by using ImageJ software (available at http://rsbweb.nih.gov/ij/). The intensities of these bands were compared to a standard curve generated with known numbers of genome copies of *in vitro* synthesized RNA from WNR C-hFLuc2A NS1-5 (ranging from 2000 to 200,000 copies), and the resulting standard curve (generated by using GraphPad Prism 4 software) (Fig. S1) was used to calculate the genome copies in each test sample. The specific infectivities of each preparation were then calculated by dividing this genome copy number per IU in the same sample volume, giving genome copies/IU of each VRP.

Western blot analyses of NS1

VRPs containing different derivatives of WNR C-hFLuc2A NS1-5 were inoculated onto BHK cell monolayers at an MOI of 5 and incubated at 37 °C with serum-free medium (OptiPro SFM, Gibco) supplemented with 10 mM HEPES and antibiotics. At 24 h after infection, culture fluids were collected and cell lysates were prepared using lysis buffer (0.1% Triton X-100, 300 mM NaCl, 50 mM Tris–HCl; pH 7.6) containing a protease inhibitor cocktail (Roche). Samples were resolved on 4–12% gradient Bis–Tris polyacrylamide gels (Invitrogen) and transferred to polyvinyldene diofluoride membranes, which were then incubated with a 1:5000 dilution of a mouse anti-NS1 antibody from hydridoma JE-6H4 (Kitai et al., 2007). Following washing, the membranes were incubated with a 1:10,000 dilution of peroxidase-conjugated anti-mouse IgG (KPL), and the bound peroxidase was visualized by using ECL Plus System (GE healthcare).

VRP focus-formation assay

To compare focus morphology, monolayers of BHK(VEErep/WNVC*-E/Pac) cells expressing the WNV C-prM-E proteins were infected with serial dilutions of VRPs harboring the WT replicon genome, or genomes encoding the NS2A^{F9F}, NS2A^{F9F}NS3^{R516K} or NS3^{R516K} mutations. Following absorption for 2 h, the cells were overlaid with medium containing 0.8% carboxymethyl cellulose (CMC) (Sigma, Saint Louis, MO) supplemented with 1% FBS, 10 mM HEPES and antibiotics and incubated at 37 °C for 48 h. To visualize foci, the cells were fixed with 50% acetone–50% methanol solution followed by incubation with a 1:5000 dilution of a mouse anti-NS1 antibody from hybridoma JE-6H4 (Kitai et al., 2007), peroxidase conjugated anti-mouse IgG (KPL, Gaithersburg, MD) and VIP substrate (Vector Laboratories, Burlingame, CA). The number of cells forming individualized focus was counted and used to compare focus size.

Luciferase assay

BHK monolayers prepared in 96-well black-wall plates were infected with dilutions of VRPs harboring the WT replicon genome, or genomes encoding the NS2A^{F9F}, NS2A^{F9F}NS3^{R516K} or NS3^{R516K} mutations and incubated at 37 °C. At 24 h post infection, an equal volume of 25% Steady-Glo Luciferase Assay System reagent (Promega) diluted in lysis buffer was added to the cells and incubated for 5 min on rocker to allow cell lysis. The luminescence was measured on a Microplate Luminometer (Applied Biosystems, Foster City, CA). A parallel plate infected with the same dilutions of VRPs was harvested at 24 h post infection and used to determine the number of VRP-infected cells determined by immunostaining (as described above). The luciferase activity was normalized by the number of VRP-infected cells and expressed as relative luciferase units (RLU) per infected cell.

Statistical analyses

GraphPad Prism (GraphPad Software, San Diego, CA) was used to analyze data. One-way or two-way analysis of variance (ANOVA) with the Bonferroni post-test were used where appropriate. P values less than 0.05 were considered to indicate statistical significance.

Acknowledgments

We thank T. Ishikawa (Kobe University) for helpful discussion concerning NS1' detection and E. Konishi (Kobe University) for supplying the JE-6H4 monoclonal antibody. This work was supported by a grant from NIAID to PWM through the Western Regional Center of Excellence for Biodefense and Emerging Infectious Disease Research (NIH grant number U54 AI057156), NIH grants R21 AI077077 and UO1 AI082960 and a grant from the Sealy Center for Vaccine Development (SCVD). ERW was supported by a SCVD Predoctoral Fellowship for a portion of these studies.

Appendix A. Supplementary data

Supplementary data to this article can be found online at doi:10.1016/j.virol.2011.09.007.

References

Alcon, S., Talarmin, A., Debruyne, M., Falconar, A., Deubel, V., Flamand, M., 2002. Enzyme-linked immunosorbent assay specific to Dengue virus type 1 nonstructural protein NS1 reveals circulation of the antigen in the blood during the acute phase of disease in patients experiencing primary or secondary infections. J. Clin. Microbiol. 40 (2), 376–381.

Anez, G., Men, R., Eckels, K.H., Lai, C.J., 2009. Passage of dengue virus type 4 vaccine candidates in fetal rhesus lung cells selects heparin-sensitive variants that result in loss of infectivity and immunogenicity in rhesus macaques. J. Virol. 83 (20), 10384–10394.

Bourne, N., Scholle, F., Silva, M.C., Rossi, S.L., Dewsbury, N., Judy, B., De Aguiar, J.B., Leon, M.A., Estes, D.M., Fayzulin, R., Mason, P.W., 2007. Early production of type I interferon during West Nile virus infection: role for lymphoid tissues in IRF3-independent interferon production. J. Virol. 81 (17), 9100–9108.

Fan, W.F., Mason, P.W., 1990. Membrane association and secretion of the Japanese encephalitis virus NS1 protein from cells expressing NS1 cDNA. Virology 177 (2), 470–476.

Fayzulin, R., Scholle, F., Petrakova, O., Frolov, I., Mason, P.W., 2006. Evaluation of replicative capacity and genetic stability of West Nile virus replicons using highly efficient packaging cell lines. Virology 351 (1), 196–209.

Firth, A.E., Atkins, J.F., 2009. A conserved predicted pseudoknot in the NS2A-encoding sequence of West Nile and Japanese encephalitis flaviviruses suggests NS1' may derive from ribosomal frameshifting. Virol. J. 6, 14.

Fonseca, B.A.L., 1994. Vaccinia-vectored dengue vaccine candidates elicit neutralizing antibodies in mice. Doctoral thesis. Yale University, New Haven, CT.

Gilfoy, F., Fayzulin, R., Mason, P.W., 2009. West Nile virus genome amplification requires the functional activities of the proteasome. Virology 385 (1), 74–84.

Halstead, S.B., Thomas, S.J., 2011. New Japanese encephalitis vaccines: alternatives to production in mouse brain. Expert Rev. Vaccines 10 (3), 355–364.

Higuchi, R., Krummel, B., Saiki, R.K., 1988. A general method of in vitro preparation and specific mutagenesis of DNA fragments: study of protein and DNA interactions. Nucleic Acids Res. 16 (15), 7351–7367.

Ishikawa, T., Widman, D.G., Bourne, N., Konishi, E., Mason, P.W., 2008. Construction and evaluation of a chimeric pseudoinfectious virus vaccine to prevent Japanese encephalitis. Vaccine 26 (22), 2772–2781.

Junjhon, J., Edwards, T.J., Utaipat, U., Bowman, V.D., Holdaway, H.A., Zhang, W., Keelapang, P., Puttikhunt, C., Perera, R., Chipman, P.R., Kasinrerk, W., Malasit, P., Kuhn, R.J., Sittisombut, N., 2010. Influence of pr-M cleavage on the heterogeneity of extracellular dengue virus particles. J. Virol. 84 (16), 8353–8358.

Kitai, Y., Shoda, M., Kondo, T., Konishi, E., 2007. Epitope-blocking enzyme-linked immunosorbent assay to differentiate West Nile virus from Japanese encephalitis virus infections in equine sera. Clin. Vaccine Immunol. 14 (8), 1024–1031.

Konishi, E., Pincus, S., Fonseca, B.A., Shope, R.E., Paoletti, E., Mason, P.W., 1991. Comparison of protective immunity elicited by recombinant vaccinia viruses that synthesize E or NS1 of Japanese encephalitis virus. Virology 185 (1), 401–410.

Kroschewski, H., Allison, S.L., Heinz, F.X., Mandl, C.W., 2003. Role of heparan sulfate for attachment and entry of tick-borne encephalitis virus. Virology 308 (1), 92–100.

Lee, E., Lobigs, M., 2000. Substitutions at the putative receptor-binding site of an encephalitic flavivirus alter virulence and host cell tropism and reveal a role for glycosaminoglycans in entry. J. Virol. 74 (19), 8867–8875.

Lee, E., Lobigs, M., 2002. Mechanism of virulence attenuation of glycosaminoglycan-binding variants of Japanese encephalitis virus and Murray Valley encephalitis virus. J. Virol. 76 (10), 4901–4911.

Lee, E., Hall, R.A., Lobigs, M., 2004. Common E protein determinants for attenuation of glycosaminoglycan-binding variants of Japanese encephalitis and West Nile viruses. J. Virol. 78 (15), 8271–8280.

Lee, E., Wright, P.J., Davidson, A., Lobigs, M., 2006. Virulence attenuation of Dengue virus due to augmented glycosaminoglycan-binding affinity and restriction in extraneural dissemination. J. Gen. Virol. 87 (Pt 10), 2791–2801.

Li, L., Lok, S.M., Yu, I.M., Zhang, Y., Kuhn, R.J., Chen, J., Rossmann, M.G., 2008. The flavivirus precursor membrane–envelope protein complex: structure and maturation. Science 319 (5871), 1830–1834.

Libraty, D.H., Young, P.R., Pickering, D., Endy, T.P., Kalayanarooj, S., Green, S., Vaughn, D.W., Nisalak, A., Ennis, F.A., Rothman, A.L., 2002. High circulating levels of the dengue virus nonstructural protein NS1 early in dengue illness correlate with the development of dengue hemorrhagic fever. J. Infect. Dis. 186 (8), 1165–1168.

Lindenbach, B.D., Rice, C.M., 1999. Genetic interaction of flavivirus nonstructural proteins NS1 and NS4A as a determinant of replicase function. J. Virol. 73 (6), 4611–4621.

Lindenbach, B.D., Theil, H.-J., Rice, C.M., 2007. *Flaviviridae*: the viruses and their replication, In: Knipe, D.M., Howley, P.M. (Eds.), Fifth ed. Fields Virology, Vol. 1. Lippincott Williams & Wilkins, Philadelphia, pp. 1101–1152. 2 vols.

Mandl, C.W., Allison, S.L., Holzmann, H., Meixner, T., Heinz, F.X., 2000. Attenuation of tick-borne encephalitis virus by structure-based site-specific mutagenesis of a putative flavivirus receptor binding site. J. Virol. 74 (20), 9601–9609.

Mason, P.W., 1989. Maturation of Japanese encephalitis virus glycoproteins produced by infected mammalian and mosquito cells. Virology 169 (2), 354–364.

Mason, P.W., Shustov, A.V., Frolov, I., 2006. Production and characterization of vaccines based on flaviviruses defective in replication. Virology 351 (2), 432–443.

Melian, E.B., Hinzman, E., Nagasaki, T., Firth, A.E., Wills, N.M., Nouwens, A.S., Blitvich, B.J., Leung, J., Funk, A., Atkins, J.F., Hall, R., Khromykh, A.A., 2010. NS1' of flaviviruses in the Japanese encephalitis virus serogroup is a product of ribosomal frameshifting and plays a role in viral neuroinvasiveness. J. Virol. 84 (3), 1641–1647.

Muylaert, I.R., Chambers, T.J., Galler, R., Rice, C.M., 1996. Mutagenesis of the N-linked glycosylation sites of the yellow fever virus NS1 protein: effects on virus replication and mouse neurovirulence. Virology 222 (1), 159–168.

Muylaert, I.R., Galler, R., Rice, C.M., 1997. Genetic analysis of the yellow fever virus NS1 protein: identification of a temperature-sensitive mutation which blocks RNA accumulation. J. Virol. 71 (1), 291–298.

Patkar, C.G., Kuhn, R.J., 2008. Yellow Fever virus NS3 plays an essential role in virus assembly independent of its known enzymatic functions. J. Virol. 82 (7), 3342–3352.

Staples, J.E., Gershman, M., Fischer, M., 2010. Yellow fever vaccine: recommendations of the Advisory Committee on Immunization Practices (ACIP). MMWR Recomm. Rep. 59 (RR-7), 1–27.

Suzuki, R., Winkelmann, E.R., Mason, P.W., 2009. Construction and characterization of a single-cycle chimeric flavivirus vaccine candidate that protects mice against lethal challenge with dengue virus type 2. J. Virol. 83 (4), 1870–1880.

Thompson, J.F., Hayes, L.S., Lloyd, D.B., 1991. Modulation of firefly luciferase stability and impact on studies of gene regulation. Gene 103 (2), 171–177.

van der Schaar, H.M., Rust, M.J., Waarts, B.L., van der Ende-Metselaar, H., Kuhn, R.J., Wilschut, J., Zhuang, X., Smit, J.M., 2007. Characterization of the early events in dengue virus cell entry by biochemical assays and single-virus tracking. J. Virol. 81 (21), 12019–12028.

Widman, D.G., Ishikawa, T., Fayzulin, R., Bourne, N., Mason, P.W., 2008. Construction and characterization of a second-generation pseudoinfectious West Nile virus vaccine propagated using a new cultivation system. Vaccine 26 (22), 2762–2771.

Youn, S., Cho, H., Fremont, D.H., Diamond, M.S., 2010. A short N-terminal peptide motif on flavivirus nonstructural protein NS1 modulates cellular targeting and immune recognition. J. Virol. 84 (18), 9516–9532.

Yu, I.M., Zhang, W., Holdaway, H.A., Li, L., Kostyuchenko, V.A., Chipman, P.R., Kuhn, R.J., Rossmann, M.G., Chen, J., 2008. Structure of the immature dengue virus at low pH primes proteolytic maturation. Science 319 (5871), 1834–1837.

THE JOURNAL OF BIOLOGICAL CHEMISTRY VOL. 286, NO. 43, pp. 37264–37273, October 28, 2011

Role of the Endoplasmic Reticulum-associated Degradation (ERAD) Pathway in Degradation of Hepatitis C Virus Envelope Proteins and Production of Virus Particles*[S]

Received for publication, May 7, 2011, and in revised form, August 18, 2011 Published, JBC Papers in Press, August 30, 2011, DOI 10.1074/jbc.M111.259085

Mohsan Saeed[§], Ryosuke Suzuki[‡], Noriyuki Watanabe[‡], Takahiro Masaki[‡], Mitsunori Tomonaga[‡], Amir Muhammad[¶], Takanobu Kato[‡], Yoshiharu Matsuura[‖], Haruo Watanabe[§], Takaji Wakita[‡], and Tetsuro Suzuki[‡‡‡1]**

*From the [‡]Department of Virology II, National Institute of Infectious Diseases, Tokyo 162-8640, Japan, the [§]Department of Infection and Pathology, Graduate School of Medicine, the University of Tokyo, Tokyo 113-0033, Japan, the [¶]Department of Pathology, Khyber Girls Medical College, Peshawar 25000, Pakistan, the [‖]Research Institute of Microbial Diseases, Osaka University, Osaka 565-0871, Japan, the **National Institute of Infectious Diseases, Tokyo 162-8640, Japan, and the [‡‡]Department of Infectious Diseases, Hamamatsu University School of Medicine, Hamamatsu 431-3192, Japan.*

Background: HCV causes ER stress in the infected cells.
Results: HCV-induced ER stress leads to increased expression of certain proteins that in turn enhance the degradation of HCV glycoproteins and decrease production of virus particles.
Conclusion: HCV infection activates the ERAD pathway, leading to modulation of virus production.
Significance: ERAD plays a crucial role in the viral life cycle.

Viral infections frequently cause endoplasmic reticulum (ER) stress in host cells leading to stimulation of the ER-associated degradation (ERAD) pathway, which subsequently targets unassembled glycoproteins for ubiquitylation and proteasomal degradation. However, the role of the ERAD pathway in the viral life cycle is poorly defined. In this paper, we demonstrate that hepatitis C virus (HCV) infection activates the ERAD pathway, which in turn controls the fate of viral glycoproteins and modulates virus production. ERAD proteins, such as EDEM1 and EDEM3, were found to increase ubiquitylation of HCV envelope proteins via direct physical interaction. Knocking down of EDEM1 and EDEM3 increased the half-life of HCV E2, as well as virus production, whereas exogenous expression of these proteins reduced the production of infectious virus particles. Further investigation revealed that only EDEM1 and EDEM3 bind with SEL1L, an ER membrane adaptor protein involved in translocation of ERAD substrates from the ER to the cytoplasm. When HCV-infected cells were treated with kifunensine, a potent inhibitor of the ERAD pathway, the half-life of HCV E2 increased and so did virus production. Kifunensine inhibited the binding of EDEM1 and EDEM3 with SEL1L, thus blocking the ubiquitylation of HCV E2 protein. Chemical inhibition of the ERAD pathway neither affected production of the Japanese encephalitis virus (JEV) nor stability of the JEV envelope protein. A co-immunoprecipitation assay showed that EDEM orthologs do not bind with JEV envelope protein. These findings highlight the crucial role of the ERAD pathway in the life cycle of specific viruses.

Quality control of proteins, such as the elimination of misfolded proteins, is largely connected with the endoplasmic reticulum (ER),[2] which is an organelle responsible for the folding and distribution of secretory proteins to their sites of action. This pathway is termed ER-associated degradation (ERAD) and is triggered by ER stress. It results in retrotranslocation of misfolded proteins into the cytosol, followed by polyubiquitylation and proteasomal degradation (1). Several viral infections have been reported to trigger the ERAD pathway (2–4); however, the role of this pathway in the life cycle of viruses remains poorly defined.

Initiation of the ERAD pathway occurs from the oligomerization and autophosphorylation of IRE1, an ER stress sensor. The activated IRE1 removes an intron from X-box-binding protein 1 (XBP1) mRNA, which then encodes a potent transcription factor for activation of genes, for example, ER degradation-enhancing α-mannosidase-like protein (EDEM). EDEM1 (5), along with its two homologs EDEM2 (6) and EDEM3 (7), as well as ER mannosidase I (ER ManI), belong to the glycoside hydrolase 47 family. EDEMs are thought to function as lectins that deliver misfolded glycoproteins to the ERAD pathway. However, the precise mechanism by which they assist in glycoprotein quality control remains unclear.

Hepatitis C virus (HCV) infection is a major cause of chronic liver disease. The RNA genome of HCV, a member of the Fla-

* This work was supported by grants-in-aid from the Ministry of Health, Labor and Welfare, and from the Ministry of Education, Culture, Sports, Science, and Technology, Japan.
[S] The on-line version of this article (available at http://www.jbc.org) contains supplemental Figs. S1–S7.
[1] To whom correspondence should be addressed: Dept. of Infectious Diseases, Hamamatsu University School of Medicine, Hamamatsu 431-3192, Japan. Tel.: 81-53-435-2336; Fax: 81-53-435-2338; E-mail: tesuzuki@hama-med.ac.jp.

[2] The abbreviations used are: ER, endoplasmic reticulum; CHX, cycloheximide; EDEM, ER degradation-enhancing α-mannosidase-like protein; ERAD, ER-associated degradation; HCV, hepatitis C virus; JEV, Japanese encephalitis virus; KIF, kifunensine; ManI, mannosidase I; m.o.i., multiplicity of infection; TM, tunicamycin; XBP1, X-box-binding protein 1; IRE, inositol-requiring enzyme.

viviridae family, encodes the viral structural proteins Core, E1, E2, and p7, as well as six nonstructural proteins (8, 9). Two *N*-glycosylated envelope proteins E1 and E2 are exposed on the surface of the virus and are necessary for viral entry.

The aim of this study was to investigate whether the ERAD pathway is activated upon HCV infection and whether this affects the quality control of virus glycoproteins and virion production. We show that HCV infection triggers the ERAD pathway, possibly through IRE1-mediated splicing of XBP1. Moreover, EDEM1 and EDEM3, but not EDEM2, interact with HCV glycoproteins, resulting in increased ubiquitylation. EDEM1 knockdown and chemical inhibition of the ERAD pathway increases glycoprotein stability, as well as production of infectious virus particles, whereas overexpression of EDEM1 decreases virion production. These results provide insight into the mechanism by which HCV triggers the ERAD pathway and subsequently affects the quality control of virus glycoproteins and virus particle production.

EXPERIMENTAL PROCEDURES

Cell Culture and Chemicals—Human hepatoma cells HuH-7 and HuH-7.5.1 (a gift from Dr. F. V. Chisari (The Scripps Research Institute) (10) and human embryonic kidney cells 293T were cultured at 37 °C and 5% CO_2 in DMEM containing 10% FBS, 10 mM HEPES, 1 mM sodium pyruvate, nonessential minimum amino acids, 100 units/ml penicillin, and 100 μg/ml streptomycin. Tunicamycin (TM) was purchased from Sigma-Aldrich, and kifunensine (KIF) was purchased from Toronto Research Chemicals (Ontario, Canada).

Preparation of Virus Stock—HCV JFH-1 was generated by introducing *in vitro* transcribed RNA into HuH-7.5.1 cells by electroporation, and virus stocks were prepared by infecting at a multiplicity of infection (m.o.i.) of 0.01, as described previously (10). Infected cells were grown in culture medium containing 2% FBS, and supernatants were collected after multiple passages to get high titer virus. The supernatants were concentrated using a 500-kDa hollow fiber module (GE Healthcare) resulting in ~90% recovery of the virus. Focus-forming units were measured with an anti-HCV core antibody to determine virus titration (2H9, described below). Virus stocks containing 1×10^7 focus-forming units/ml were divided into small aliquots and stored at −80 °C until use. rAT strain of Japanese encephalitis virus (JEV) (11) was used to generate virus stock.

Plasmids—cDNAs of mouse EDEM1-HA, EDEM2, and EDEM3-HA, having 92, 93, and 91% amino acid homology with their human orthologs, respectively, were a kind gift from Drs. N. Hosokawa (Kyoto University) and K. Nagata (Kyoto Sangyo University). A HA tag was attached to the C terminus of EDEM2 by PCR, and sequencing analysis was performed to confirm the sequence. To generate pJFH/E1dTM-myc and pJFH/E2dTM-myc, HCV E1 encoding amino acids 170–352 and HCV E2 encoding amino acids 340–714 of JFH-1 polyprotein were amplified by PCR with forward primer and reverse primer containing NotI and XbaI restriction sites, respectively, and cloned into a NotI/XbaI site of the pEF1/Myc-His plasmid (Invitrogen). The pCAGC105E plasmid carrying PrM and E proteins of the rAT strain of JEV has been described (12). Plasmids carrying the firefly luciferase reporter gene under control of the intact promoter of GRP78 and GRP94 or the defective promoter lacking ERSE elements have been described (13) and were a kind gift from Dr. K. Mori (Kyoto University).

Antibodies—Rabbit polyclonal antibodies included anti-HA (Sigma-Aldrich), anti-HCV NS5A (14), anti-SEL1L (Sigma-Aldrich), anti-ubiquitin (MBL, Nagoya, Japan), and anti-JEV E antibodies. The mouse monoclonal antibodies were anti-HA (clone 16B12; Covance, Emeryville, CA), anti-HCV E2 (clone 8D10-3),[3] anti-β-actin (clone AC15; Sigma-Aldrich), anti-HCV core (clone 2H9) (15), and anti-Myc (clone 9E10; Santa Cruz Biotechnology, Santa Cruz, CA) antibodies. Anti-JEV antibodies have been described (16) and were a kind gift from Drs. C. K. Lim and T. Takasaki (National Institute of Infectious Diseases).

Analysis of XBP1 Splicing—Total RNA was extracted from cells using Isogen (Nippon Gene, Tokyo, Japan) following the manufacturer's protocol, and 2 μg of RNA was subjected to cDNA synthesis using oligo(dT) and Superscript III (Invitrogen). PCR was carried out using specific primers 5′-AAACAGAGTAGCAGCTCAGACTGC-3′ and 5′-GTATCTCTAAGACTAGGGGCTTGGTA-3′ for XBP1 and 5′-TCCTGTGGCATCCACGAAACT-3′ and 5′-GAAGCATTTGCGGTGGACGAT-3′ for β-actin to generate PCR fragments of 598 bp for unspliced XBP1, 572 bp for spliced XBP1, and 315 bp for β-actin. The following cycling conditions were used to amplify the genes: 1 cycle of 98 °C for 3 min, followed by 30 cycles of 98 °C for 20 s, 55 °C for 30 s, and 72 °C for 1 min, followed by a final extension of 72 °C for 10 min. The PCR product of XBP1 was further digested with PstI enzyme (New England Biolabs) and resolved on a 2% agarose gel prepared in TAE buffer. Unspliced XBP1 yielded two smaller fragments of 291 and 307 bp whereas spliced XBP1 stayed intact due to loss of the restriction site after splicing.

Gene Microarray Analysis—For microarray analysis, RNA was extracted from HuH-7.5.1 cells at 48 and 72 h after JFH-1 infection. Cells treated for 12 h with 5 μg/ml TM served as a positive control. Hybridization was performed on a 3D-Gene (see 3D-Gene web site) Human Oligonucleotide chip 25k (Toray Industries Inc., Tokyo, Japan). For efficient hybridization, this microarray chip has three dimensions and is constructed with a well between the probes and cylinder stems with 70-mer oligonucleotide probes on the top. Total RNA was labeled with Cy3 or Cy5 using the Amino Allyl MessageAMP II aRNA Amplification kit (Applied Biosystems). The Cy3- or Cy5-labeled aRNA pools were subjected to hybridization for 16 h using the supplier's protocol. Hybridization signals were scanned using a ScanArray Express Scanner (PerkinElmer Life Sciences) and processed by GenePixPro version 5.0 (Molecular Devices, Sunnyvale, CA). Detected signals for each gene were normalized using a global normalization method (Cy3/Cy5 ratio median = 1). Genes with Cy3/Cy5 normalized ratios $>\log_2 1.0$ or $<\log_2 -1.0$ were defined, respectively, as significantly up- or down-regulated genes.

Quantification of Cellular Gene Expression—Gene expression levels were measured using predesigned assay-on-demand (Applied Biosystems). RT-PCR amplification was performed

[3] D. Akazawa, N. Nakamura, and T. Wakita, unpublished data.

under the following conditions: 48 °C for 30 min, 95 °C for 10 min, 50 cycles of 95 °C for 15 s, and 60 °C for 1 min. Standard curves were constructed on a 1:5 serial dilution of the RNA template. The results were normalized to GAPDH mRNA levels.

Determination of Protein Stability—HuH-7 cells were infected with HCV JFH-1 at a m.o.i. of 2. Six hours after infection, the cells were either treated with KIF or transfected with EDEM1 siRNA. Forty hours later, culture medium was replaced with 100 μg/ml cycloheximide (CHX). Cells, including floating cells, were harvested at different time points after CHX addition, and immunoblotting was performed to determine the amount of HCV E2.

Plasmid Transfection and Immunoprecipitation—HuH-7 or 293T cells were seeded in 6-well cell culture plates at 3×10^5 cells/well and cultured overnight. Plasmid DNA was transfected into cells using TranIT-LT1 transfection reagent (Mirus, Madison, WI). Cells were harvested at 48 h after transfection, washed once with 1 ml of PBS, and lysed in 200 μl of lysis buffer (20 mM Tris-HCl, pH 7.4, 135 mM NaCl, 1% Triton X-100, and 10% glycerol supplemented with 50 mM NaF, 5 mM Na_3VO_4, and protease inhibitor mixture tablets (Roche Diagnostics). Cell lysates were sonicated at 4 °C for 10 min, incubated for 30 min at 4 °C, and centrifuged at 14,000 × *g* for 5 min at 4 °C. After preclearing for 2 h, the supernatants were immunoprecipitated overnight by rotating with 1.5 μl of anti-HA monoclonal antibody (16B12) or anti-HCV E2 monoclonal antibody (clone 8D10-3) at 4 °C. The immunocomplexes were then captured on protein G-agarose beads (Invitrogen) by rotation-incubation at 4 °C for 3 h. Beads were subsequently precipitated by centrifugation at 800 × *g* for 1 min and washed five times with lysis buffer. Finally, proteins bound to the beads were boiled in 40 μl of SDS sample buffer and subjected to SDS-PAGE.

Western Blotting—Proteins resolved by SDS-PAGE were transferred onto PVDF membranes (Immobilon; Millipore). After blocking in 2% skim milk, the membranes were probed with primary antibodies followed by exposure to peroxidase-conjugated secondary antibodies and visualization with an ECL Plus Western blotting detection system (GE Healthcare). The intensity of the bands was measured using a computerized imaging system (ImageJ software; National Institutes of Health).

Small Interfering RNA (siRNA) Transfection—HuH-7 cells were transfected with duplex siRNAs at a final concentration of 10 nM using Lipofectamine RNAiMAX (Invitrogen). Three siRNAs for each gene were examined for knock-down efficiency and cytotoxic effects. The siRNA with best performance was selected for further experiments. Target sequences of the siRNAs which exhibited the best knock-down efficiencies were as follows: EDEM1 (sense) 5′-CAUAUCCUCGGGUGAAUCUtt-3′, EDEM2 (sense) 5′-GAAUGUCUCAGAAUUCCAAtt-3′, EDEM3 (sense) 5′-CAUGAGACUACAAAUCUUAtt-3′, IRE1 (sense) 5′-GGACGUGAGCGACAGAAUAtt-3′. 5′-GGUGUCCUUACCAUACUAAtt-3′ served as a negative control. The lowercase letters denote overhanging deoxyribonucleotides.

Quantification of HCV Core and RNA—HCV core was quantified using an enzyme immunoassay (Ortho HCV antigen ELISA kit; Ortho Clinical Diagnostics, Tokyo, Japan). HCV RNA was quantified as described (17).

Statistical Analysis—Student's *t* test was employed to calculate the statistical significance of the results. $p < 0.05$ was considered significant.

RESULTS

HCV Infection Induces XBP1 mRNA Splicing and EDEM Expression—XBP1 plays a key role in activating the ERAD pathway, which mediates unfolded protein response in the ER. Under conditions of ER stress, XBP1 mRNA is processed by unconventional splicing and translated into functional XBP1, which in turn mediates transcriptional up-regulation of a variety of ER stress-dependent genes. The resultant activation of downstream pathways boosts the efficiency of ERAD, which coincides with elevated transcription of EDEMs. To validate our method for detecting activation of the ERAD pathway, we exposed HuH-7.5.1 cells to TM, which is a typical ER stress inducer, and performed an assay to quantify spliced XBP1 mRNA, as described under "Experimental Procedures," at different time points after treatment. The spliced form of XBP1 mRNA started accumulating within these cells as early as 2 h after exposure to TM (Fig. 1*A*), and levels remained elevated until at least 12 h after treatment. Quantitative RT-PCR showed that mRNA levels of EDEM1, EDEM2, and EDEM3 were elevated in TM-treated cells whereas ER ManI, which is not an ER stress-responsive gene, did not show any up-regulation (Fig. 1*B*). To examine involvement of the ERAD pathway in the HCV life cycle, we infected HuH-7.5.1 cells with JFH-1 at m.o.i. of 5 and analyzed XBP1 mRNA splicing and EDEM up-regulation. Upon infection, the fragment corresponding to spliced XBP1 mRNA, was detectable 8 h after infection, and the difference in splicing between mock- and HCV-infected cells became more pronounced at 48 h after infection and then persisted (Fig. 1*C*). Increased levels of XBP1 mRNA splicing were dependent on the m.o.i. (supplemental Fig. 1*A*), suggesting that expression of active XBP1 was induced by HCV infection. A small amount of spliced XBP1 was detected in mock-infected cells, presumably because of some intrinsic stress. A 3.1-fold increase in the level of EDEM1 mRNA was observed at 3–4 days after infection ($p < 0.05$). Increases in EDEM2 and EDEM3 mRNA levels were moderate and reached ~1.5-fold, whereas ER ManI mRNA exhibited no change after infection (Fig. 1*D*). Expression of EDEMs, particularly EDEM1, was up-regulated in accordance with HCV infection titers (supplemental Fig. 1*B*). Knocking down the IRE1 gene (Fig. 1*E*) effectively reversed the accumulation of spliced XBP1, as well as the transcriptional up-regulation of EDEM1 (Fig. 1*F*), thus confirming that HCV infection induces ERAD through the IRE1-XBP1 pathway.

To enable a comprehensive investigation of the transcriptional changes that occur, up- and down-regulation of the transcriptome was examined in HCV-infected cells and in TM-treated cells. The results were compared with those of mock-transfected cells at each time point. A range of genes involved in ER stress was found to be regulated in HCV-infected and in TM-treated cells (Fig. 2*A*). EDEM1 was signifi-

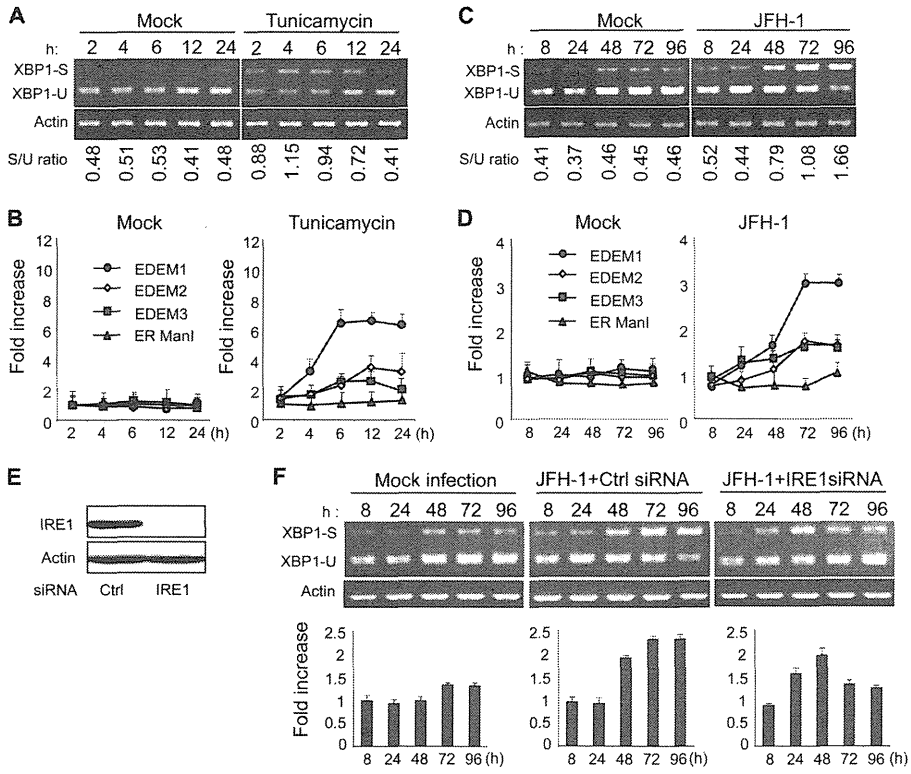

FIGURE 1. **Splicing of XBP1 mRNA and induction of ERAD gene expression in HCV JFH-1-infected cells.** *A*, splicing of XBP1 mRNA analyzed in mock- and TM (5 μg/ml)-treated HuH-7.5.1 cells at different time points after treatment. The *upper* and *lower bands* represent spliced and unspliced RNA, respectively. The *numbers* at the *bottom* of the *panel* indicate the density ratios of bands corresponding to spliced and unspliced XBP1. *B*, graphs showing the -fold induction of EDEM1, EDEM2, EDEM3, and ER Man1 mRNA in HuH-7.5.1 cells treated or untreated with TM. Data are normalized to GAPDH expression levels. The mean ± S.D. (*error bars*) of three independent experiments are shown. *C*, splicing of XBP1 mRNA analyzed in mock- and HCV JFH-1-infected HuH-7.5.1 cells (m.o.i. 5) at different time points after infection. *Numbers* at the *bottom* of the *panel* indicate the density ratios of bands corresponding to spliced and unspliced XBP1. *D*, real-time PCR analysis of EDEM1, EDEM2, EDEM3, and ER ManI mRNA induction in mock- and HCV-infected cells. Data are normalized to GAPDH expression. The mean ± S.D. of three independent experiments are shown. Note that a reduction in the level of GAPDH mRNA within infected cells was not observed until 96 h after infection when a slight decrease was observed. This led us to use GAPDH as a housekeeping gene in our experiments. *E*, Western blotting of IRE1 in cells transfected with mock or gene-specific siRNA of IRE1. *F*, splicing of XBP1 mRNA and induction of EDEM1 in HCV-infected cells after knocking down of the IRE1 gene. HuH-7.5.1 cells infected with JFH-1 at a m.o.i. of 5 were transfected with mock (*center*) or IRE1-specific siRNA (*right*) 48 h after infection, after which splicing of XBP1 (*upper*) and transcriptional up-regulation of EDEM1 (*lower*) were examined at the indicated time points after infection. The mean ± S.D. of two independent experiments are shown.

cantly up-regulated upon HCV infection, whereas expression levels of EDEM2 and EDEM3 remained unchanged. Although transcriptional changes caused by HCV infection in many of the genes listed are analogous to those that occur in cells treated with TM, up-regulation of two ER chaperone proteins, GRP78 and GRP94, was induced by TM treatment but not by HCV infection. This differential induction was confirmed by a reporter assay for GRP78 promoter and GRP94 promoter activities (Fig. 2*B*). These results are in agreement with a previously described finding that GRP78 and GRP94 are not responsive to HCV infection in hepatoma cells (18). It remains likely that HCV infection interferes with transcriptional activation of some ER chaperone proteins; however, the mechanism by which this occurs remains to be elucidated.

EDEMs Cause Ubiquitylation of HCV Glycoproteins and Enhance Their Degradation—Because EDEMs have been reported to enhance proteasomal degradation of ERAD substrates through direct binding, we investigated the interaction of EDEMs with HCV glycoproteins in 293T cells by co-transfecting the expression plasmids for E1dTM or E2dTM together with plasmids carrying either EDEM or ER ManI genes. Immunoprecipitation and immunoblotting demonstrated that each EDEM, but not ER ManI, was capable of interacting with E2 (Fig. 3*A*) and E1 (supplemental Fig. S2). HCV glycoproteins displayed enhanced mobility when co-expressed with EDEM1, EDEM3, or ER ManI, which could be due to the mannosidase activity of these proteins, which is lacking in EDEM2 (6). HCV primarily replicates in hepatocytes so we examined the interaction of EDEMs with E2dTM in HuH-7 cells as well, which yielded similar results (data not shown). E2dTM lacks the transmembrane domain, which could affect its folding and ER retention and thus modulate the ability of this protein to interact with EDEMs and ER ManI. Second, E1 and E2 glycoproteins assemble as noncovalent heterodimers to make functional complexes, which may alter the interaction of these proteins with EDEMs. To address these issues, we co-transfected HuH-7 cells with plasmids carrying full-length E1E2 glycoproteins together with plasmids carrying either EDEMs or ER ManI. Similar phenotypes were produced following transfection full-length E1E2 proteins (supplemental Fig. S3*A*), demonstrating that functional complexes of HCV glycoproteins bind with EDEMs. Recently, we have reported on the development of a

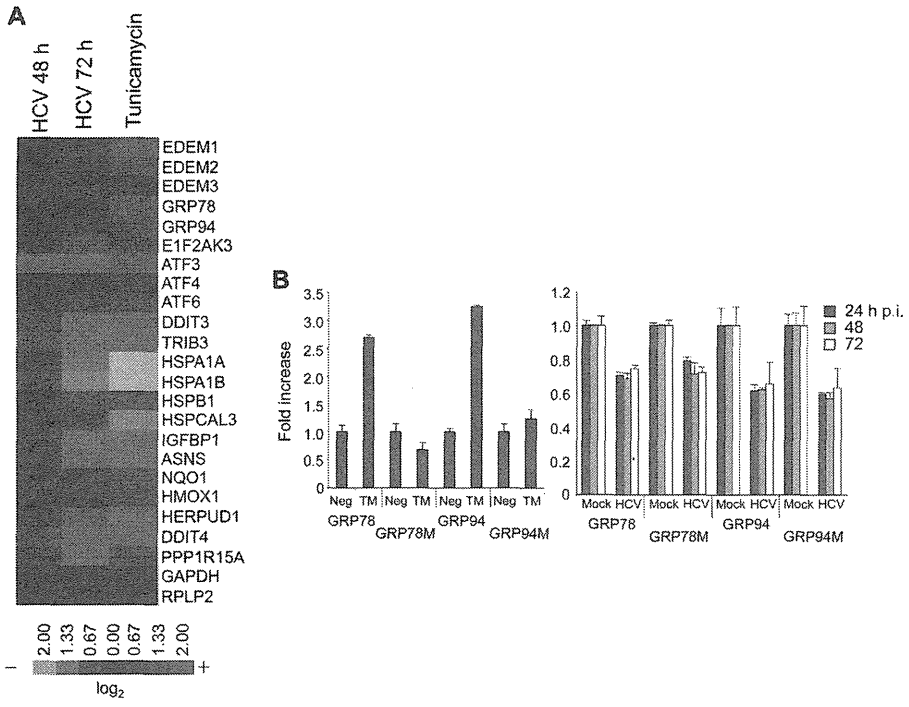

FIGURE 2. **Comprehensive analysis of ERAD gene expression in JFH-1-infected HuH-7.5.1 cells.** *A*, HuH-7.5.1 cells treated with TM (5 μg/ml) for 12 h or infected with JFH-1 for 48 and 72 h were subjected to microarray analysis, along with their negative controls. Expression of ER stress genes is shown as a heat map. *Red* and *green* indicate up- and down-regulation, respectively. Information on each gene shown is indicated on the 3D-Gene web site. *B*, GRP78 and GRP94 induction in TM-treated (*left*) and HCV-infected cells (*right*). GRP78M and GRP94M represent the defective promoters. The mean ± S.D. (*error bars*) of three independent experiments are shown.

packaging system of HCV subgenomic replicon sequences through the provision of viral core NS2 proteins in *trans* (19). Transcomplementation with core NS2 proteins resulted in successful packaging of the viral sequences; therefore, plasmids carrying these proteins are a valid construct by which to examine the interaction of envelope proteins with ERAD machinery. Thus, we performed an immunoprecipitation assay of HuH-7 cells co-transfected with core NS2 and EDEMs. In agreement with our previous results, EDEMs, but not ER ManI, were observed to bind to HCV E2 protein (supplemental Fig. S3*B*). To examine the functional importance of this interaction, we analyzed the ubiquitylation of HCV E2 protein in cells co-transfected with HCV E2 and EDEM proteins. An immunoprecipitation assay revealed that overexpression of EDEM1 and EDEM3, but not of EDEM2 and ER ManI, dramatically increased the ubiquitylation of HCV glycoprotein (Fig. 3*B*). In mammals, the ER membrane ubiquitin-ligase complex involved in the dislocation of ERAD substrates, and their ubiquitylation contains the ER membrane adaptor SEL1L. It has recently been shown that SEL1L interacts with EDEM1 in cells and functions as a cargo receptor for ERAD substrates (20); however, it is unknown whether SEL1L interacts with other EDEMs. We therefore assessed whether SEL1L interacts with EDEM1, EDEM2, EDEM3, and ER ManI in cells (Fig. 3*C*). Interestingly, endogenous SEL1L co-precipitated with EDEM1 and EDEM3, whereas little to no interaction was observed with EDEM2 and ER ManI. Collectively, it is likely that, although all EDEMs can recognize HCV E1 and E2, EDEM1 and EDEM3 are involved in the ubiquitylation of HCV glycoproteins by delivering them to SEL1L-containing ubiquitin-ligase complexes. To investigate further the role of EDEMs in quality control of HCV glycoproteins, we measured the steady-state level of HCV E2 protein after EDEM knockdown. Transfection of HCV-infected cells with siRNAs against EDEM1, EDEM2, or EDEM3 caused a 60–80% reduction in mRNA levels of the respective genes (Fig. 3*D*) with no cytotoxic effects observed (data not shown). Immunoblotting showed a considerable increase in the steady-state level of viral E2 in EDEM1 siRNA-treated cells (Fig. 3*D*). We subsequently examined the turnover of E2 in cells with and without EDEM1 knockdown. In CHX half-life experiments, E2 protein was moderately unstable in control-infected cells, presumably via proteasomal degradation (Fig. 3*E*). Treatment with MG132, a proteasome inhibitor, blocked its destabilization (data not shown). In contrast, E2 was completely stable in EDEM1-knockdown cells during the chase period of time tested (Fig. 3*E*). Together, these results strongly suggest that EDEM1 and EDEM3, particularly EDEM1, are involved in the post-translational control of HCV glycoproteins.

Involvement of EDEM1 in the Production of Infectious HCV—Given the involvement of EDEMs in the turnover of HCV glycoproteins, we investigated whether EDEMs affect the replication and production of infectious virus particles. EDEMs were knocked down in HCV-infected HuH-7 cells by siRNA transfection, and the production of infectious particles was then monitored by measuring the extracellular infectivity titer. Knocking down of EDEM1 and EDEM3 in the infected cells resulted in ~3.1-fold ($p < 0.05$) and ~2.3-fold increases in virus production, respectively, compared with control cells. No effect

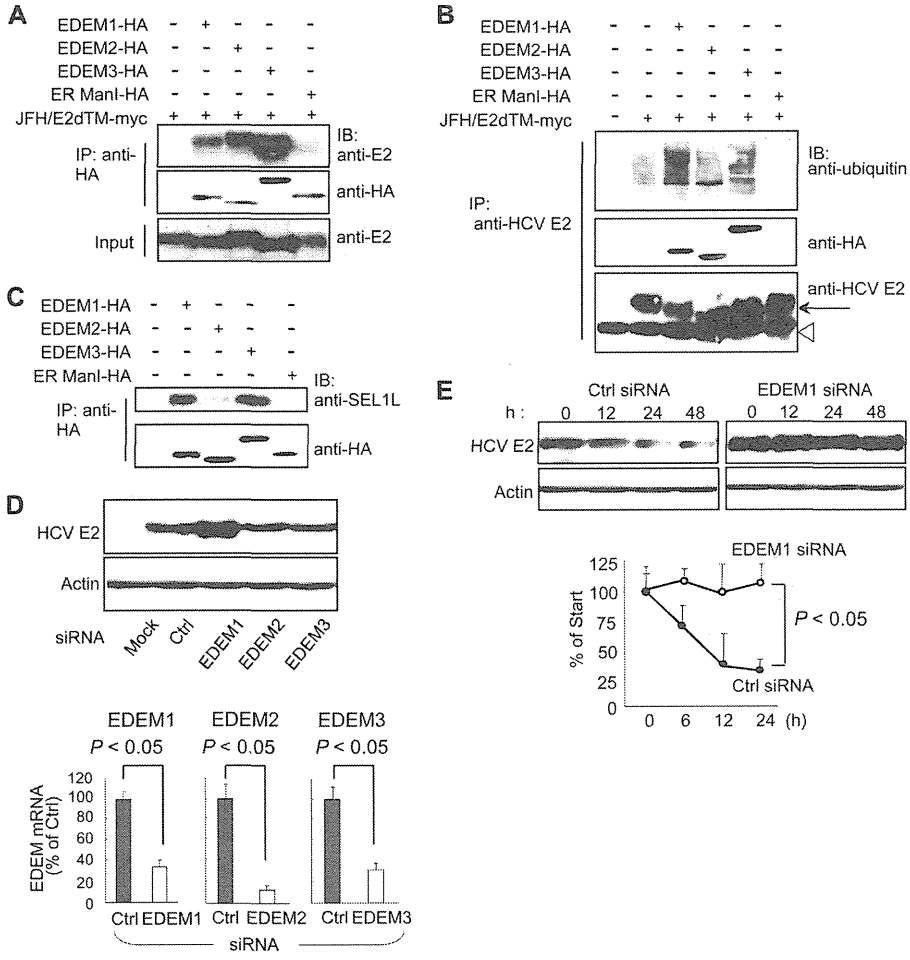

FIGURE 3. **EDEMs are involved in the degradation of HCV glycoproteins.** *A*, binding of EDEMs and ER ManI with HCV E2. 293T cells were seeded in 6-well plates at a density of 3×10^5 cells/well. After overnight incubation, cells were co-transfected with plasmids carrying HCV E2-myc (1 μg) and EDEM1-HA, EDEM2-HA, EDEM3-HA, or ER ManI-HA proteins (1 μg each). Forty-eight hours later, cells were harvested, immunoprecipitated (*IP*) with anti-HA antibodies, and Western blotting (*IB*) was performed with the indicated antibodies. *B*, ubiquitylation of HCV E2 protein in cells co-transfected with HCV E2 and EDEM plasmids. 293T cells were seeded in 6-well plates at a density of 3×10^5 cells/well. Twenty-four hours later, the cells were co-transfected with plasmids carrying HCV E2-myc (1 μg) and EDEM1-HA, EDEM2-HA, EDEM3-HA, or ER ManI-HA genes (1 μg each). Forty-eight hours later, the cells were harvested and immunoprecipitated with anti-E2 antibodies, and Western blotting was performed with the indicated antibodies. *Arrow*, HCV E2; *open arrowhead*, immunoglobulin heavy chain. *C*, binding of EDEMs and ER ManI with endogenous SEL1L in cells. *D*, steady-state level of HCV E2 in HCV-infected HuH-7 cells after EDEM knockdown (*upper*). The knockdown efficiencies of the respective siRNAs are shown in the *lower panel*. Values are normalized to GAPDH expression levels, and normalized values in negative control cells have been arbitrarily set at 100%. *E*, stability of HCV E2 protein in EDEM1 knockdown cells. HCV-infected HuH-7 cells were transfected with control or EDEM1 siRNA. Forty hours later, the cells were exposed to CHX (100 μg/ml) for 0, 12, 24, and 48 h, followed by immunoblotting. Specific signals were quantified by densitometry, and the percent of HCV E2 remaining was compared with initial levels. The mean ± S.D. (*error bars*) of two independent experiments are shown.

on virus production was observed following EDEM2 gene silencing (Fig. 4*A*). On the other hand, no significant differences were observed with regard to intracellular HCV core protein levels among mock- and EDEM siRNA-transfected cells (Fig. 4*B*), which indicates that replication of the viral genome is not affected by EDEM proteins. To examine further whether this effect on virus production was due to turnover of HCV envelope proteins, we performed loss-of-EDEM-function experiments in HuH-7 cells carrying HCV subgenomic replicons. Because the replicons do not require envelope proteins, they should be insensitive to the expression levels of genes involved in the ERAD pathway. As expected, siRNA-mediated knockdown of EDEMs resulted in little to no change in genome replication (supplemental Fig. S4*A*). To investigate further the participation of EDEMs in the HCV life cycle, HCV-infected cells were examined 48 h after transfection with an expression plasmid for either EDEM1, EDEM2, or EDEM3. As expected, exogenous expression of EDEM1 in the infected cells led to a 2.4-fold decrease in virus production compared with mock-transfected cells ($p < 0.05$) (Fig. 4*C*). A moderate decrease of 1.7-fold was observed in the cells overexpressing EDEM3 protein. Ectopic expression of EDEMs and ER ManI did not cause any change in intracellular HCV core protein levels (Fig. 4*D*). Similarly, little or no change was observed in genome replication when plasmids carrying EDEMs were introduced into HCV subgenomic replicon cells (supplemental Fig. S4*B*). These results indicate that EDEM1 and EDEM3, particularly EDEM1, regulate virus production, possibly through post-translational control of HCV glycoproteins.